Article

Developmental Cell

Plk4 Regulates Centriole Asymmetry and Spindle Orientation in Neural Stem Cells

Graphical Abstract

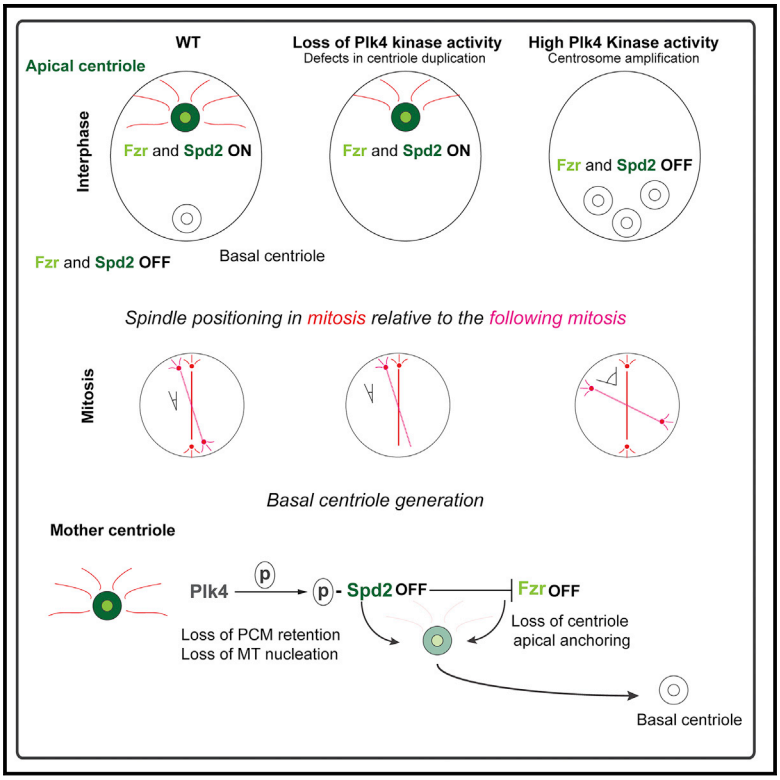

Highlights

- *Drosophila* Plk4 mutant NSCs show defects in centriole asymmetry and spindle positioning
- Apical centriole anchoring requires the PCM protein Spd-2 and the APC/C activator Fzr
- Movement of the centriole toward the basal side of the cell requires Plk4 activity
- At the mother centriole, Plk4 phosphorylates Spd2 to trigger PCM shedding and Fzr loss

Authors

Davide Gambarotto, Carole Pennetier, John M. Ryniawec, ..., Yuu Kimata, Gregory C. Rogers, Renata Basto

Correspondence

gcrogers@email.arizona.edu (G.C.R.), renata.basto@curie.fr (R.B.)

In Brief

Mitotic spindle orientation is tightly regulated during development and adulthood to maintain tissue organization and homeostasis. Spindle orientation requires the coordination between centrosomes and cortical cues. Gambarotto et al. report that the centrosome components Plk4 and Spd2 regulate centrosome asymmetry in interphase to influence spindle positioning in mitosis.

Gambarotto et al., 2019, Developmental Cell *50*, 11–24
July 1, 2019
https://doi.org/10.1016/j.devcel.2019.04.036

CellPress

Developmental Cell
Article

Plk4 Regulates Centriole Asymmetry and Spindle Orientation in Neural Stem Cells

Davide Gambarotto,[1,5] Carole Pennetier,[1] John M. Ryniawec,[2] Daniel W. Buster,[2] Delphine Gogendeau,[1] Alix Goupil,[1] Maddalena Nano,[1] Anthony Simon,[1] Damien Blanc,[3] Victor Racine,[3] Yuu Kimata,[4] Gregory C. Rogers,[2,*] and Renata Basto[1,6,*]

[1]Institut Curie, PSL Research University, CNRS, UMR144, Biology of centrosomes and Genetic instability lab, Paris 75005, France
[2]Department of Cellular and Molecular Medicine, University of Arizona Cancer Center, University of Arizona, Tucson, AZ 85724, USA
[3]QuantaCell, 2 Allée du Doyen Georges Brus, Pessac 33600, France
[4]School of Life Science and Technology, ShanghaiTech University, 393 Middle Huaxia Road, Pudong, Shanghai, 201210, China
[5]Present address: University of Geneva, Department of Cell Biology, Sciences III, Geneva, Switzerland
[6]Lead Contact
*Correspondence: gcrogers@email.arizona.edu (G.C.R.), renata.basto@curie.fr (R.B.)
https://doi.org/10.1016/j.devcel.2019.04.036

SUMMARY

Defects in mitotic spindle orientation (MSO) disrupt the organization of stem cell niches impacting tissue morphogenesis and homeostasis. Mutations in centrosome genes reduce MSO fidelity, leading to tissue dysplasia and causing several diseases such as microcephaly, dwarfism, and cancer. Whether these mutations perturb spindle orientation solely by affecting astral microtubule nucleation or whether centrosome proteins have more direct functions in regulating MSO is unknown. To investigate this question, we analyzed the consequences of deregulating Plk4 (the master centriole duplication kinase) activity in *Drosophila* asymmetrically dividing neural stem cells. We found that Plk4 functions upstream of MSO control, orchestrating centriole symmetry breaking and consequently centrosome positioning. Mechanistically, we show that Plk4 acts through Spd2 phosphorylation, which induces centriole release from the apical cortex. Overall, this work not only reveals a role for Plk4 in regulating centrosome function but also links the centrosome biogenesis machinery with the MSO apparatus.

INTRODUCTION

Drosophila neural stem cells (NSCs; also called neuroblasts [NBs]) repeatedly divide asymmetrically to self-renew and to generate a committed progenitor, the ganglion mother cell (GMC). During interphase, a robust mechanism of centriole asymmetry controls mitotic spindle orientation (MSO) in the following mitosis (Rebollo et al., 2007; Rusan and Peifer, 2007) so that GMCs are always born at the same position relative to the NB (Figure 1A). Defects in polarity establishment or mutations in centrosome genes, which disrupt spindle positioning, interfere with asymmetric cell division and generate tumors (Basto et al., 2008; Basto et al., 2006; Castellanos et al., 2008; Caussinus and Gonzalez, 2005), highlighting the importance of regulated stem cell division.

The stereotypical asymmetric centriole behavior in NBs described previously (Rebollo et al., 2007; Rusan and Peifer, 2007) largely contributes to the fidelity of asymmetric cell divisions. Within a centrosome, centrioles have different ages, and they can be structurally and/or functionally different (Conduit et al., 2015). This asymmetry is strongly visible during mitotic exit, just after disengagement of the mother-daughter centriole pair. The daughter or younger centriole retains microtubule (MT) nucleation activity, forming an aster that anchors the centriole to the apical cell cortex (hereafter called the apical centriole) (Rebollo et al., 2007; Rusan and Peifer, 2007; Conduit et al., 2010; Januschke and Gonzalez, 2010). In contrast, the mother or older centriole becomes inactivated and loses MT nucleation capacity, resulting in displacement away from the apical cortex toward the basal side (hence, referred to as basal centriole). Thus, the daughter centriole is retained in the NB, while the mother centriole is inherited by the GMC (Conduit et al., 2010; Januschke et al., 2011).

The discrepancy in the ability to nucleate MTs by the two centrioles can be explained by differences in pericentriolar material (PCM) retention (Conduit et al., 2010; Januschke et al., 2013). Maintenance of Polo kinase at the daughter centriole is crucial in retaining its PCM. Both positive and negative regulatory mechanisms control Polo localization on centrioles (Januschke et al., 2013; Ramdas Nair et al., 2016; Lerit and Rusan, 2013; Singh et al., 2014). The basal centriole is inactivated through ''PCM shedding,'' consisting of the rapid downregulation of the PCM (Rebollo et al., 2007; Rusan and Peifer, 2007), which is mediated by Plp and Bld10 (*Drosophila* orthologs of Pericentrin and Cep135, respectively) (Lerit and Rusan, 2013; Singh et al., 2014).

Although past studies have been instrumental in dissecting the molecular machinery responsible for asymmetric centriole behavior and the consequent impact on the MSO, the mechanisms responsible for centriole asymmetry establishment are not fully understood. Here, we uncover a function for Polo-like kinase 4 (Plk4), the master regulator of centriole duplication, in the establishment of this asymmetry. We show that Spd2 is a Plk4 substrate and that Spd2 phosphorylation triggers a basal-like centriole behavior. Furthermore, we found that the centriolar protein Fzr (the anaphase promoting complex [APC/C] activator

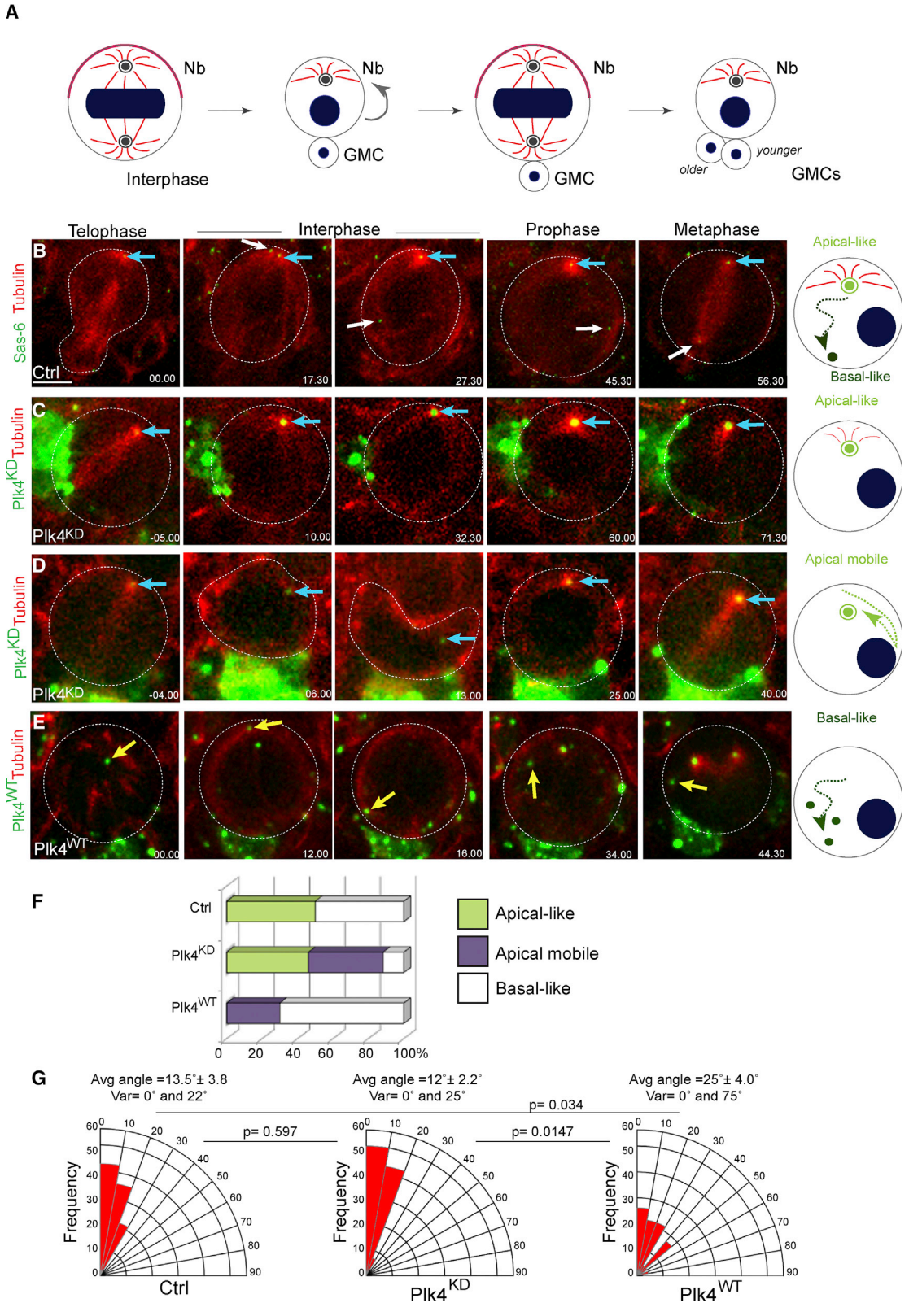

(legend on next page)

and the ortholog of Cdh1 in vertebrates) functions as a positive apical centriole retention factor in NBs. Our work provides evidence of a role for centrosome proteins in orchestrating centrosome asymmetry and MSO.

RESULTS

Altering Plk4 Activity Perturbs the Centrosome Asymmetry Cycle and Causes Spindle Positioning Defects

Drosophila NBs display a robust pattern of centriole asymmetry, which controls MSO and ensures that GMCs are always born at the same position relative to the NB (Figure 1A) (Rebollo et al., 2007; Rusan and Peifer, 2007) as confirmed by our time-lapse analysis of wild-type (WT) NBs (referred to as Control [Ctrl]) (n=20 Ctrl NBs from 8 brains) (Figures 1B and 1F; Video S1).

While analyzing the division of NBs expressing a GFP-tagged kinase-dead version of Plk4 (referred to as Plk4^{KD}; Figure S1) in the Plk4 mutant (Plk4^{mut}) background, we observed an unexpected behavior. The unduplicated centriole was preferentially maintained at the apical side in 88.5% of Plk4^{KD} NBs (n = 23 out of 26 NBs from 7 brains). Of these, 46.2% contained an immobile centriole (Figures 1C and 1F; Video S2A) that remained apically anchored throughout interphase. In 46.3% of Plk4^{KD} NBs, this centriole was maintained at an apical position even if it presented increased mobility. In this situation, the centriole movement was restricted to the apical hemisphere, the centriole moved from one side of the cell to the other (hereafter, referred to as apical mobile) (Figures 1D and 1F; Video S2A). Interestingly, in the example of Figure 1D and Video S2C, even if the apical cortex was deformed by a neighboring cell, the centriole was maintained at an apical position with little variation from one cell cycle to the following one. In the remaining 11.5% Plk4^{KD} NBs, centrioles moved toward the basal side of the cell as described for basal centriole behavior (referred to as basal-like) (n = 3 out of 26 NBs from 7 brains) (data not shown; Figure 1F). Importantly, even if containing a single centriole, all Plk4^{KD} NBs assembled a bipolar spindle. Initially, MT nucleation was noticed in the pole that contains the centriole; but rapidly, a bipolar array was generated, and cells invariably divided in a bipolar manner, similar to cells that lack centrioles (Basto et al., 2006; Moutinho-Pereira et al., 2009). These observations were very surprising because it is expected that as the unduplicated centriole ages, it should show a basal-like behavior, as shown by older mother centrioles (Figure S2A). The retention of the unduplicated centriole in NBs was also described in Plk4^{mut} NBs where a significant number of NBs contain a single centriole (Bettencourt-Dias et al., 2005).

To ascertain the behavior of an unduplicated centriole that was generated using a different centriole duplication mutant background, we counted centrioles in NBs of Sas-4^{mut} brains and compared these with Plk4^{KD} and Plk4^{mut} brains. *Drosophila* harboring mutations in key centriole genes are viable because of maternally provided centriole assembly factors that ensure centriole duplication during early embryogenesis when centrosomes are essential (Stevens et al., 2007; Basto et al., 2006; Riparbelli and Callaini, 2011; Bettencourt-Dias et al., 2005; Blachon et al., 2008). As development proceeds, centriole duplication ends around stage 15 or 16 (Basto et al., 2006) however, centrioles born prior to this stage are stably maintained. As cells continue to proliferate and increase in number throughout development, centrioles are detected in only a small number of cells. Indeed, a single centriole was detected in only 2.2% ± 1.4% of Sas-4^{mut} NBs (n = 305 NBs from 7 brains) (Figure S2C). Moreover, we could not find centrioles in dividing NBs by live imaging of Sas-4^{mut} brains (Figure S2D). In contrast, a single centriole was detected in 38.9% ± 5.6% of Plk4^{mut} and 62.4% ± 15.4% of Plk4^{KD} NBs (n = 187 NBs from 5 Plk4^{mut} brains and n = 132 NBs from 5 Plk4^{KD} brains) (Figure S2C). Importantly, the Plk4 mutant used in our study is a hypomorph (Bettencourt-Dias et al., 2005), explaining why some Plk4^{mut} NBs contain centrioles at this developmental stage. Additionally, Plk4^{KD} over-expression in the Plk4^{mut} background might lead to a partial stabilization of the endogenous Plk4 protein, resulting in supernumerary centrosomes, which were detected at a low frequency (4.0% ± 5.2%) (Figure S2C). The presence of extra centrosomes, even in a small subset of cells, might contribute to an increased number of Plk4^{KD} NBs with centrioles. Thus, our analysis of the behaviors of single centrioles in Plk4^{KD} NBs suggests that loss of Plk4 activity promotes the apical cortical anchoring of an unduplicated centriole.

We next examined the consequence of over-expressing active Plk4 (referred to as a Plk4^{WT}) on centriole positioning in NBs (Figure S1A). Over-expression of Plk4 generated a large number of NBs with extra centrosomes (78.1%; n = 274 NBs from 6 brains) (Figure S2C) (Basto et al., 2008; Habedanck et al., 2005; Marthiens et al., 2013). Surprisingly, however, and in contrast to Plk4^{KD} NBs, centrioles in the majority of Plk4^{WT} NBs displayed basal-like movement (70%; n = 14 of 20 NBs from 7 brains) (Figures 1E and 1F; Video S2C). Additionally, these centrioles did not produce detectable interphase MT asters, similarly to basal centrioles in Ctrl NBs. In the remaining 30% of Plk4^{WT} NBs, centrioles presented apical mobile behavior with either a reduced MT aster (10%) or without a noticeable MT aster (20%) (n = 2 and n = 4 of 20 NBs from 7 brains, respectively). The lack of an apical centriole in Plk4^{WT} NBs was unforeseen as at least

Figure 1. Plk4 Regulates Centriole Dynamics in Interphase, Impacting Spindle Orientation

(A) Schematic drawing representing two consecutive cell cycles of a *Drosophila* NB depicting centrosome behavior.

(B–E) Images from time-lapse movies of Ctrl (B), Plk4^{KD} (C and D), and Plk4^{WT} (E) larval NBs. Tubulin in red. RFP-Sas-6 (B), GFP-Plk4^{KD} (C and D), and GFP-Plk4^{WT} (E) in green. See also Figures S1 and S2. The blue arrow denotes the centrosome (or centriole in the case of Plk4^{KD}) inherited by the NB at the end of mitosis in the first column but, in all other images, marks the centriole that was localized at the apical cortex (apical centriole) after disengagement. White arrows point to the centriole that moves basally in Ctrl NBs. The yellow arrow points to the centrosome positioned at the spindle pole at the end of mitosis in Plk4^{WT} NBs. Time, minutes. Scale, 4 μm. Diagrams on the right illustrate centriole behavior in early interphase.

(F) Graph shows the percentage of centriole behavior categories during interphase in the indicated genotypes. Centriole behavior was categorized as apical-like in (B) or (C), apical-mobile-like in (D), when the centrosome moved laterally even if remained localized within the apical hemisphere, or basal-like in (E).

(G) Quantification of the angle between two consecutive mitoses in Ctrl, Plk4^{KD} and Plk4^{WT}. Statistical significance (SS) was assessed by unpaired t test.

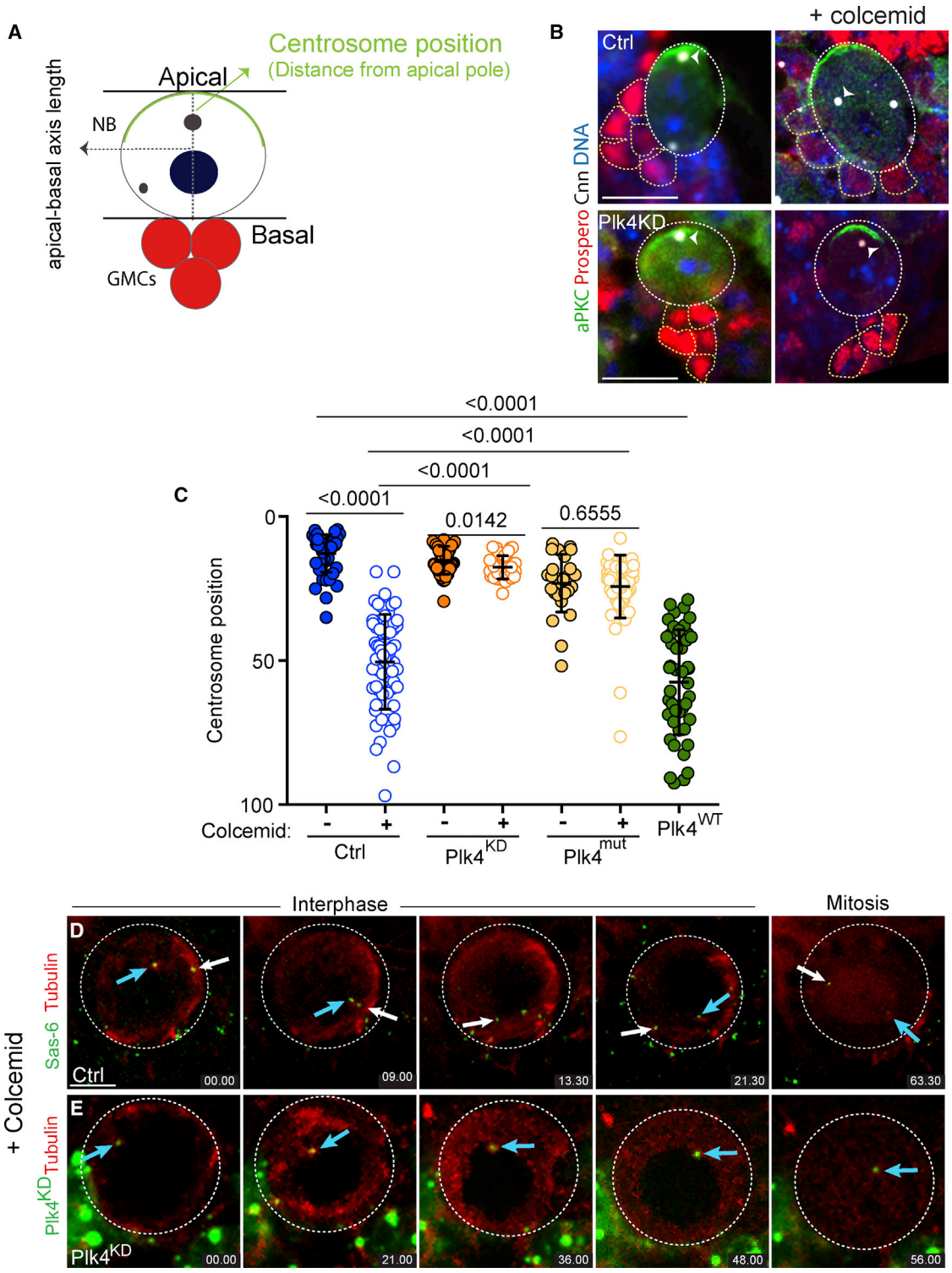

Figure 2. The Single Centriole of Plk4^{KD} NBs Does Not Behave as in Ctrl NBs after MT Depolymerization

(A) Schematic drawing of NBs with a hypothetic apical basis length (dashed line). Position zero was considered the apical cortex, while position 100 at the basal cortex was determined by its connection with GMCs.

(B) Immunostaining of Ctrl (top) and Plk4^{KD} (bottom) NBs and GMCs with (right) or without (left) colcemid treatment with antibodies against aPKC and Prospero in green and red, respectively. The centrosome is labeled with Cnn antibodies (white) and DNA in blue. The apical centrosome in Ctrl NBs was recognized by containing a higher Cnn signal (white arrowhead). Scale: Ctrl, 3 μm; and Plk4KD, 4 μm. See also Figure S3.

(legend continued on next page)

one of the young centrioles is predicted to maintain an apical localization during interphase.

Since the asymmetric centriole cycle controls MSO over several NB divisions (Rebollo et al., 2007; Rusan and Peifer, 2007), we investigated the consequences of $Plk4^{KD}$ or $Plk4^{WT}$ expression in MSO. We filmed Ctrl, $Plk4^{KD}$, and $Plk4^{WT}$ NBs over at least two consecutive mitoses and found that spindles in $Plk4^{KD}$ NBs maintained a fixed position, similar to Ctrl NBs (average angle = 13.5° ± 3.8°; variation between 0° and 22°; n = 15 NBs from 8 brains for $Plk4^{KD}$ and average angle = 12.0° ± 2.2°; variation between 0° and 25°; n = 14 NBs from 3 brains for Ctrl; p = not significant (ns); Figure 1G). In contrast, $Plk4^{WT}$ NBs displayed a more variable MSO through consecutive cycles (average angle = 25.0° ± 4.0°; variation between 0° and 75°; n = 23 from 10 brains; p = 0.026; Figure 1G). Characterization of MSO relative to the polarity axis using atypical protein kinase C (aPKC) as a marker (Lee et al., 2006; Homem and Knoblich, 2012) showed that in Ctrl NBs, spindles were oriented along the polarity axis (average angle = 9.9° ± 0.7°; variation between 2.3° and 45°; n = 48 NBs from 4 brains) (Figures S3A and S3B). In $Plk4^{KD}$, the average angle was slightly increased to 15.3° ± 1.2° (variation between 5.4° and 60.9°; n = 62 NBs from 5 brains; p = 0.013) showing that even if the unduplicated centriole tends to maintain apical localization during interphase, mitotic spindles do not orient as correctly as Ctrl NBs. Importantly, in $Plk4^{WT}$ NBs, the average angle was increased to 23.5° ± 2.1° (variation between 3.9° and 89.6°; n = 96 NBs from 7 brains; p < 0.0001) (Figures S3A and S3B), confirming that increased Plk4 activity influences apical centrosome positioning in interphase and, thus, MSO. Defects in MSO can lead to defects in asymmetric cell division leading to the generation of two NBs instead of one NB and one GMC (Albertson and Doe, 2003; Basto et al., 2006; Basto et al., 2008; Castellanos et al., 2008; Homem and Knoblich, 2012). Using Dead pan (Dpn) (San-Juan and Baonza, 2011) as an NB marker, we determined the average number of NBs in the central brain lobe of Ctrl brains (48.9 ± 0.9; n = 9 brain lobes), similarly to previous studies (Basto et al., 2008; Gogendeau et al., 2015). Importantly, an increase in the number of NBs was noticed in $Plk4^{WT}$ central brain (55.2 ± 1.0; n = 9 brain lobes; p = 0.0003). Taken together, our results indicate that Plk4 activity must be tightly regulated not only to ensure the formation of a single procentriole per mother but also to control MSO and asymmetric cell division in NBs.

An MT-Independent Mechanism Contributes to Apical Centriole Maintenance in $Plk4^{KD}$ NBs

While characterizing $Plk4^{KD}$ NBs, we realized that the apical aster appeared to have decreased MT nucleation when compared to Ctrl NBs (Figures 1C and 1D; Videos 1 and 2), suggesting that a yet unidentified mechanism might contribute to centriole anchoring in this cell type. To further test this possibility, we treated Ctrl and $Plk4^{KD}$ brains with colcemid to depolymerize MTs for 1 h. After fixation, we used two different conditions to label NBs and centrosomes. First, NBs were identified by aPKC and GMCs by Prospero. In this case, only a centrosome marker (Cnn) was used (Figure 2A). In the second method, we used two centrosomal antibodies, Plp and Cnn, which is important to unambiguously identify centrosomes, in particular in centrosome mutants. NBs and accompanied GMCs were labeled with phalloidin, and their respective identity was determined by their size (Figure S3C). In Ctrl NBs treated with colcemid, centrosomes were closer to the basal axis as expected (Januschke and Gonzalez, 2010), reaching positions similar to the ones found in $Plk4^{WT}$ NBs (Figures 2B, 2C, S3D, and S3E). Although centrioles were further away from the apical axis in colcemid-treated $Plk4^{KD}$ NBs, they were not positioned closer to the basal hemisphere as observed in Ctrl NBs. This was also the case in $Plk4^{mut}$ NBs, suggesting that the absence of active Plk4 delays or inhibits movement toward the basal side of the cell. Consistent with these findings, time-lapse imaging revealed that centrioles in $Plk4^{KD}$ NBs treated with colcemid appeared less mobile than centrioles from colcemid-treated Ctrl brains (n = 16 NBs from 3 brains for each condition) (Figures 2D and 2E; Videos S3A and S3B). These results indicate that an alternative mechanism, which seems to be MT-independent, contributes to centriole apical anchoring in $Plk4^{KD}$ NBs.

Fzr Contributes to Anchoring of Apical Centrioles

In order to explain the apical localization of unduplicated centrioles in $Plk4^{KD}$NBs, we next immunostained NBs for centriole (Asterless [Asl]) and PCM (γ-tubulin, Spd2, and Cnn) proteins and used three-dimensional structural illumination microscopy (3D SIM) to characterize potential structural changes. Of these, Spd2 localization appeared the most distinct in centrioles from $Plk4^{KD}$ NBs (Figure 3A; data not shown). Spd2 is the *Drosophila* ortholog of Cep192, a major PCM component (Dix and Raff, 2007; Conduit et al., 2014). During interphase, Spd2 appeared as a ring in Ctrl NBs (Figure 3A) (Fu and Glover, 2012; Meghini et al., 2016; Mennella et al., 2012). In $Plk4^{KD}$ NBs, Spd2 appeared as a larger ring, while centrioles from $Plk4^{WT}$ NBs displayed a smaller Spd2 diameter (Figure 3A).

Spd2 was recently shown to recruit the APC/C activator Fizzy-related (Fzr) to the centrosome at the end of mitosis (Meghini et al., 2016). We thus investigated whether the differences in Spd2 localization in $Plk4^{KD}$ or $Plk4^{WT}$ NBs impacted Fzr levels on interphase centrioles. We generated flies expressing Red Fluorescent Protein (RFP)-Fzr (referred to as Fzr). 3D SIM images showed that Fzr occupied the internal region of the Spd2 ring (Figure 3A), as previously described (Meghini et al., 2016). In $Plk4^{KD}$ NBs, Spd2 formed an enlarged ring, and Fzr occupied

(C) Dot plot showing the position of centrosomes in Ctrl, $Plk4^{KD}$, and $Plk4^{mut}$ NBs with (+) and without (−) colcemid and $Plk4^{WT}$ NBs (Ctrl − 12.73 ± 0.9; Ctrl + 50.4 ± 0.9; $Plk4^{KD}$ − 15.17 ± 0.7; Plk4KD + 17.6 ± 0.6; $Plk4^{mut}$ − 23.14 ± 1.9; $Plk4^{mut}$ + 24.27 ± 1.5; and $Plk4^{WT}$ − 57.5 ± 2.8). Error bars represent means ± SD from at least 3 independent experiments where at least 35 NBs were analyzed from at least 8 brains. SS was assessed by unpaired t test.

(D and E) Images from time-lapse movies of Ctrl (E) and $Plk4^{KD}$ (F) NBs incubated with colcemid. The blue arrow marks the apical centriole after disengagement. The white arrow marks the basal centriole in Ctrl NBs. Time, minutes. Centrosome or centriole fluorescence intensity decreases in both Ctrl and $Plk4^{KD}$ NBs in conditions where MTs were depolymerized. This decrease is apparent as cells re-enter the following mitosis. Their dynamics and movement were followed by increasing the intensity levels, although this is not shown in the stills. Importantly, centrosomes and centrioles remain as stable structures in conditions of MT depolymerization since they can be readily noticed in immunostaining experiments using centriole and PCM markers (Figure 2C). Scale, 4 μm.

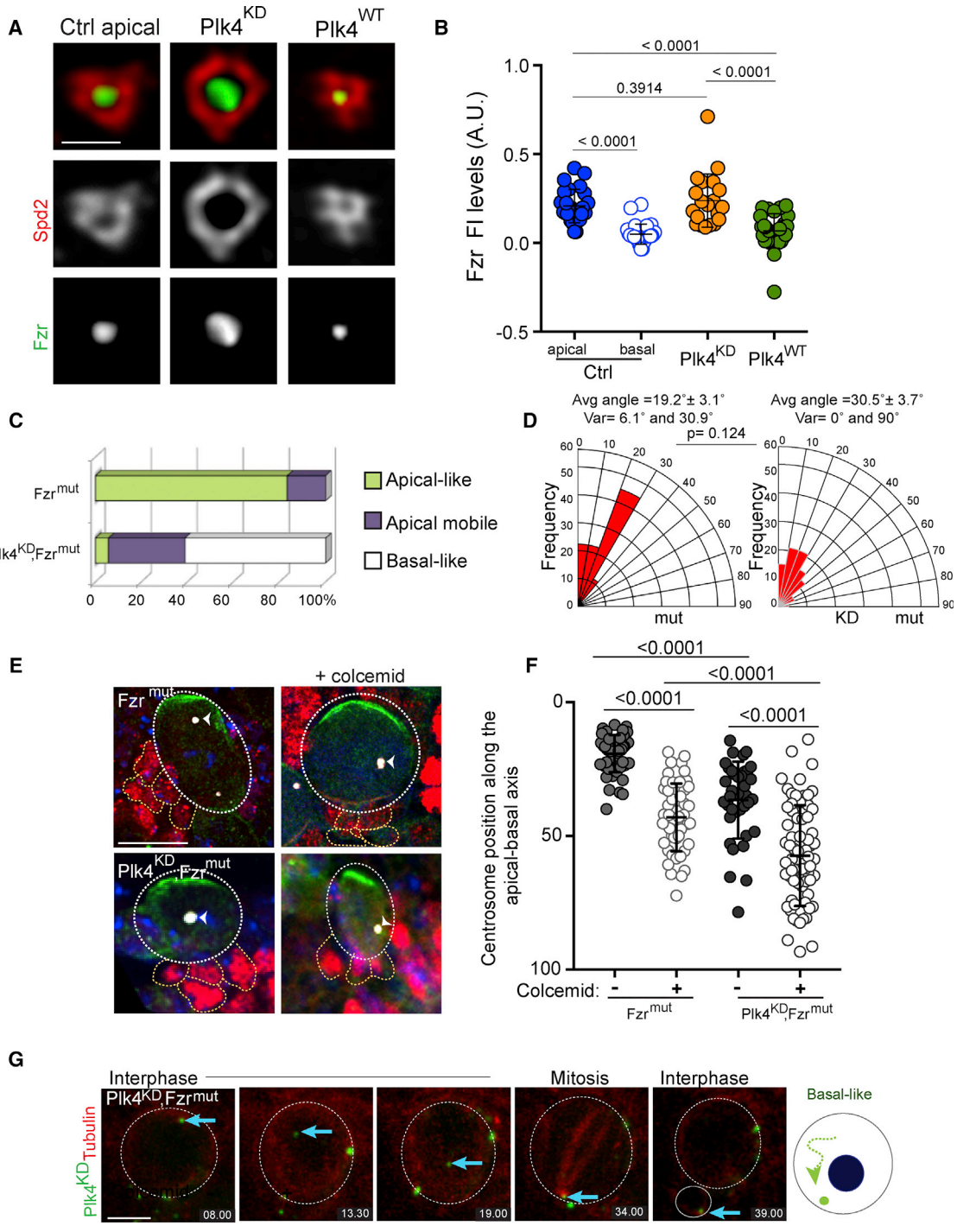

Figure 3. Maintenance of Apical Anchoring in Plk4^{KD} NBs Is Fzr Dependent

(A) 3D SIM images showing Spd2 (red) and Fzr (green) localization on interphase centrioles in Ctrl, Plk4^{KD} and Plk4^{WT} NBs. Scale, 400 nm.

(B) Dot plot showing Fzr fluorescent intensity levels at the centrosome (Ctrl apical, 0.20 ± 0.02; Ctrl basal, 0.04 ± 0.01; Plk4^{K}D, 0.24 ± 0.03; Plk4^{WT}, 0.07 ± 0.02). Error bars represent means ± SD from at least 3 independent experiments. SS was assessed by unpaired t test. See also Figure S4.

(C) Graph shows the percentage of centriole behavior categories in interphase (compare with Figure 1F for Ctrl and Plk4^{KD}).

(D) Quantification of the angle between two consecutive mitoses in Fzr^{mut} and Plk4^{KD}, Fzr^{mut}. SS was assessed by unpaired t test.

(E) Immunostaining of Fzr^{mut} and Plk4KD, Fzr^{mut} NBs and GMCs with or without colcemid treatment labeled with antibodies against aPKC and Prospero in green and red, respectively. The centrosome was labeled with Cnn antibodies (white) and DNA in blue. The apical centrosome in Fzr^{mut} NBs was recognized by containing higher Cnn signal (white arrowhead). Scale for Ctrl, 4 μm. Note that on the Fzr^{mut} panel with colcemid, the two centrosomes are very close to each other. See also Figure S5.

(legend continued on next page)

a broader area, while in Plk4^{WT} NBs, Fzr occupied a smaller area. Using images from confocal microscopy, we quantified Fzr fluorescent intensity levels at the centrioles of interphase NBs. Apical centrioles from Ctrl NBs and centrioles from Plk4^{KD} NBs contained higher Fzr levels than basal centrioles from Ctrl NBs and Plk4^{WT} centrioles (Figure 3B).

We confirmed these observations by analyzing Fzr localization using time-lapse microscopy. At the end of mitosis, Fzr was recruited to the centrosome in Ctrl NBs but exclusively remained associated with the apical centriole (Figure S4A). Fzr was also recruited to the single centriole at the end of mitosis in Plk4^{KD} NBs and to Plk4^{WT} centrioles (Figure S4A) however, its levels diminished on Plk4^{WT} interphase centrioles. These results demonstrate not only that Fzr displays an asymmetric centriolar distribution in interphase NBs but also that Plk4 activity contributes to the removal of Fzr from centrioles during interphase.

To investigate whether Fzr plays a role in establishing centrosome asymmetry, we used a hypomorphic Fzr mutant (Fzr^{mut}), which presents an overall reduction in Fzr levels (Jacobs et al., 2002). Using time-lapse microscopy of GFP-tubulin-expressing NBs in Fzr^{mut} brains, we analyzed the position of the apical MT aster. 80% of Fzr^{mut} NBs displayed apical centriole positioning (n = 16 out of 20 NBs from 4 brains) (Figure 3C), and a near-normal MSO was maintained over consecutive cycles (average angle = 19.2° ± 3.1°; variation between 6.1° and 30.9°; n = 9 NBs from 3 brains; Figure 3D). Fzr^{mut} NBs displayed normal centrosome numbers (n = 70 NBs from 4 brains) (Figure S2C). Interestingly, 20% of Fzr^{mut} NBs displayed an apical mobile behavior (Figures 3C and S4D). We also analyzed Fzr^{mut} brains after colcemid treatment and found that centrosomes were positioned closer to the basal hemisphere (Figures 3E, 3F, S3E, and S3F). It is noteworthy that in untreated conditions, Fzr^{mut} centrosomes were positioned further away from the apical cortex than Ctrl centrosomes (compare Figures 2C and 3F with Figures S3D and S3F). Taken together, our results suggest that Fzr may contribute to apical centrosome anchoring in NBs by acting in synergy with the MT nucleation pathway.

We next reasoned that decreasing Fzr levels in Plk4^{KD} NBs, which have reduced MT nucleation, should induce basal-like behavior. Importantly, very few Plk4^{KD}, Fzr^{mut} flies reached the third instar larvae stage, suggesting that combining these two mutations perturbs development. Nevertheless, we were able to obtain larvae for these studies. Remarkably, decreasing Fzr levels in Plk4^{KD} NBs induced movement of the unduplicated centriole toward the basal side in 61.1% of NBs (n = 11 of 18 NBs from 5 brains; p = 0.0009 compared to Plk4^{KD}) (Figures 3C and 3G). Additionally, 33.3% of Plk4^{KD}, Fzr^{mut} NBs (n = 6 of 18) fell into the apical mobile category, and only one Plk4^{KD},Fzr^{mut} NB maintained an apical centriole at the apical cortex during interphase (Figure 3C). Moreover, the average angle of Plk4^{KD}, Fzr^{mut} NBs was increased (Figure 3D) when compared to Fzr^{mut} and, more importantly, when compared to Plk4^{KD} NBs, (average angle = 30.5° ± 3.7°; variation between 0° and 90°; n = 32 NBs from 8 brains; p = 0.0013 relative to Plk4^{KD}; and p = 0.124 relative to Fzr^{mut}). Strikingly, colcemid treatment of Plk4^{KD}, Fzr^{mut} NBs caused centrosomes to reposition more toward the basal hemisphere (Figures 3E, 3F, S3E, and S3F). Thus, our findings suggest that Fzr participates in an MT-independent centriole apical anchoring mechanism, which is particularly active with reduced functional Plk4.

Fzr is an activator of APC/C, an E3 ubiquitin ligase that promotes mitotic exit and progression through G1 (Sivakumar and Gorbsky, 2015). Our results indicate that Fzr regulates centrosome asymmetry and, consequently, MSO. However, it remains to be investigated whether this function requires proteasome-mediated degradation of an APC/C ubiquitination target. To investigate this question, we characterized the localization of Cdc27, a core APC/C subunit, in Ctrl NBs (Huang and Raff, 2002). Although GFP-Cdc27 was slightly enriched at the centrosome at the end of mitosis, this localization was rather transient and, during interphase, GFP-Cdc27 appeared evenly distributed throughout the cytoplasm (Figure S4E). These observations reveal that APC/C is not at the centrosome at the right time to control apical anchoring. To rule out a role for APC/C in promoting apical anchoring, we tested whether inhibiting proteasomal degradation had an effect on centriole behavior by incubating Ctrl brains with Bortezomib (BZ), a proteasome inhibitor (Adams et al., 1998). Importantly, all NBs analyzed (n = 8 brains) maintained a stably anchored apical centriole, similar to controls (Figures S4F and S4G). The conditions we used increased the percentage of prometaphase-arrested NBs (41.4%; n = 7 brains) when compared to Ctrl brains incubated with DMSO (22.6%; n = 8 brains; p = 0.0433), validating the use of BZ as a proteasome inhibitor in *Drosophila* brains. Taken together, these results suggest that Fzr contributes to apical centriole anchoring and centrosome asymmetry independent of APC/C activity. Thus, retention of Fzr at the apical centriole constitutes a distinct mechanism that contributes to asymmetric cell division independent of MTs and APC/C activity.

We also asked whether an actin-based structure could contribute to apical centriole anchoring. Indeed, actin filament nucleation at the centrosome has recently been shown to occur in certain cell types (Farina et al., 2016; Obino et al., 2016). However, even if fine sub-apical actin structures could be detected, these were not co-localizing with centrosomes, and so we think that they could not be responsible for apical centriole anchoring in Ctrl or Plk4^{KD} NBs (Figure S5A). Further, we depolymerized filamentous actin (F-actin) using cytochalasin D. This treatment resulted in cytokinesis inhibition, confirming the effect of actin depolymerization. Interestingly, both Ctrl and Plk4^{KD} NBs showed a modification of the MT cytoskeleton where ectopic cytoplasmic nucleation sites were noticed (Figures S5B). Nevertheless, the apical centriole remained apically localized at the cortex throughout interphase. Thus, actin does not seem to play a role in maintaining the centriole at the apical cortex during interphase.

(F) Dot plot showing the position of centrosomes in Fzr^{mut} and Fzr^{mut},Plk4^{KD} NBs with (+) and without (−) colcemid (Fzr^{mut} − 19.26 ± 0.9; Fzr^{mut} + 43.1 ± 1.8; Fzr^{mut},Plk4^{KD} − 36.6 ± 2.3; Fzr^{mut},Plk4KD + 57.4 ± 2.2). At least 27 NBs were analyzed for each condition from 8 different brains. Error bars represent SD. SS was assessed by unpaired t test. See also Figure S3.

(G) Images from time-lapse movies of Plk4^{KD}, Fzr^{mut} NBs. Tubulin (red) and GFP-Plk4^{KD} (green). Blue arrow marks the centriole initially positioned in the NB, but later inherited by the GMC (right). Diagram illustrates centriole behavior in interphase. Time, minutes. Scale, 4 μm.

Plk4 Phosphorylates Spd2 to Promote a Basal-like Behavior

To understand how Plk4 could promote centriole asymmetry, we next focused on Spd2 because of its unique redistribution on centrosomes in response to Plk4 activity. Measurements of Spd2 fluorescence intensity levels on interphase centrosomes in Ctrl NBs revealed that its distribution appeared asymmetric, with high levels on the apical centriole and lower levels on the basal (Figures 4A and 4B). In contrast, Spd2 levels were extremely reduced in the majority of Plk4^{WT} centrioles, displaying basal-like values.

We next explored whether Plk4 regulates centrosome asymmetry through Spd2 by testing whether Spd2 is a Plk4 substrate. We found that Plk4 phosphorylated Spd2 *in vitro*, and, using tandem mass spectrometry, 28 phosphorylated Ser and Thr residues within Spd2 were identified (Figures S6A–S6D). To test the functional relevance of these modifications *in vivo*, we generated flies expressing RFP-tagged Spd2 as either WT (Spd2^{WT}) or phosphomutant transgenes, including phosphomimetic Spd2 harboring 28 aspartic acid or glutamic acid substitutions (Spd2^{DE}) and a non-phosphorylatable alanine mutant (Spd2^{AA}) (Figure S1B), all under the control of the same promoter and inserted on the same chromosome locus. The expression of Spd2 transgenes seemed to be comparable in brain extracts (Figure S6E). We then analyzed the behavior of Spd2^{WT} and Spd2 phosphomutant-expressing NBs by time-lapse microscopy in order to observe centriole behaviors and analyze MSO over consecutive mitoses. As expected, over-expression of Spd2^{WT} produced proper centrosome asymmetry, whereby an apical aster appeared after centriole disengagement (Figure 4C; Video S4A). As with endogenous Spd2, Spd2^{WT} was not detected at the basal centriole soon after disengagement until just before the following mitosis, while it remained associated with the apical centrosome. Interestingly, we also observed reduced MT nucleation, suggesting that over-expression of Spd2 might change the nucleation capacity of interphase centrosomes. Importantly, MSO was maintained with relatively small variation (average angle = 13.8° ± 7.5°; variation between 7.0° and 28.0°; n = 10 NBs from 4 brains) (Figure 4F), indicating that over-expressing Spd2^{WT} does not impact spindle positioning through consecutive cell cycles.

Despite localizing to the centrosome at the end of mitosis, Spd2^{DE} levels decreased in a similar manner from both centrioles soon after their disengagement (Figure 4D; Video S4B). Interestingly, a fixed apical centrosome was not detected throughout most interphase, and both centrioles recruited Spd2^{DE} with similar kinetics during late G2 and prophase. Importantly, in Spd2^{DE} NBs, we measured a highly variable MSO over two consecutive mitoses (average angle = 41.8° ± 20.6°; variation between 7° and 69°; n = 11 NBs from 4 brains; $p < 0.0007$ when compared to Spd2^{WT}) (Figure 4F).

We next examined the distribution of Spd2^{AA}. Similar to Spd2^{WT} and Spd2^{DE}, Spd2^{AA} localized to centrosomes at the end of mitosis. However, unlike Spd2^{WT}, Spd2^{AA} was maintained on both centrioles throughout a period of interphase (Figure 4E; Video S4C). Centrosome asymmetry was nevertheless established but much later, supporting the view that establishment of Spd2 asymmetry on centrioles relies, at least initially, on its phosphorylation state. In some NBs, the apical centriole was maintained at the apical cortex but frequently displayed an apical mobile behavior, while the other centriole also remained in the apical hemisphere (Figure 4E). Spd2^{AA} expression caused slightly more variation in MSO than Spd2^{WT} (average angle = 21.2° ± 8.9°; variation between 7° and 47°; n = 13 NBs from 5 brains; p = 0.09; ns, when compared to Spd2^{WT}), but not as dramatic as Spd2^{DE} (p = 0.0051 when compared to Spd2^{DE}) (Figure 4F).

We investigated whether replacement of the 28 phospho-residues within Spd2 in both Spd2 phosphomutants (Spd2^{DE} and Spd2^{AA}) was affecting its ability to homodimerize or interact with Cnn (Galletta et al., 2016; Conduit et al., 2014). We depleted endogenous Spd2 from S2 cells by targeting its 3′ UTR and then transiently co-expressed various combinations of Spd2^{WT}, Spd2^{DE}, and Spd2^{AA} tagged with either GFP or V5 (Figure S6E). Anti-GFP immunoprecipitations (IPs) from S2 cell lysates showed that V5-tagged Spd2^{DE} and Spd2^{AA} phosphomutants self-associate (Figure S6G). Moreover, V5-Cnn co-IPed with each of the GFP-Spd2 phosphomutants (Figure S6H), showing that the 28-amino-acid substitutions in the non-phosphorylatable and phosphomimetic Spd2 mutants do not cause protein misfolding or affect Cnn binding.

We also investigated whether Cnn centrosomal localization was influenced by the Spd2 phosphorylation state. A marked asymmetry in Cnn levels was observed between the apical and basal centrioles in Spd2^{WT} NBs (Figures 5A and 5B). Although quite variable, Cnn was still recruited to Spd2^{DE} and Spd2^{AA} NBs, suggesting that Cnn is recruited to interphase centrioles regardless of the Spd2 phosphorylation status. We also measured the levels of Plp. Plp was still preferentially enriched in the basal centrioles of Spd2^{WT} NBs and in one of the two centrioles in the Spd2 phosphomutants, even if displaying higher levels in Spd^{AA} than in Spd2^{WT} (Figures 5A and 5C).

We next measured centrosomal levels of Spd2 using anti-Spd2 antibodies (Dix and Raff, 2007). Notably, in both Spd2^{DE} and Spd2^{AA} NBs, Spd2 levels on centrosomes appeared more symmetric than centrioles in Spd2^{WT} NBs (Figures 5D and 5E). In addition, Spd2 levels on Spd2^{AA} centrosomes were comparable with Spd2^{WT} apical centrosomes, while they were decreased in Spd2^{DE} (Figure 5D).

Since Spd2 recruits Fzr to the centrosome (Meghini et al., 2016) and Fzr participates in centriole apical anchoring, we hypothesized that Fzr localization and/or levels might be altered in Spd2 phosphomutant NBs. Fzr showed asymmetric localization soon after centriole disengagement in Spd2WT NBs (Figures 5D and 5F; noticeable by the short distance between the two centrioles). Strikingly, Fzr levels were decreased in both centrioles of Spd2^{DE} NBs, suggesting that Spd2 phosphorylation impacts Fzr recruitment or maintenance in interphase centrioles. Interestingly, in Spd2^{AA} NBs, Fzr was present on both centrioles even when they were positioned far apart from one another (Figures 5D), suggesting that Fzr is maintained at both centrioles long after disengagement. Fzr asymmetry between even the two centrioles was noticeable although less pronounced than in Spd2^{WT} NBs (Figure 5F). Our findings suggest that Plk4 phosphorylation of Spd2 downregulates Spd2 and Fzr recruitment to centrioles, thereby controlling centriole asymmetry and dynamics and, consequently, MSO in the following cell cycle.

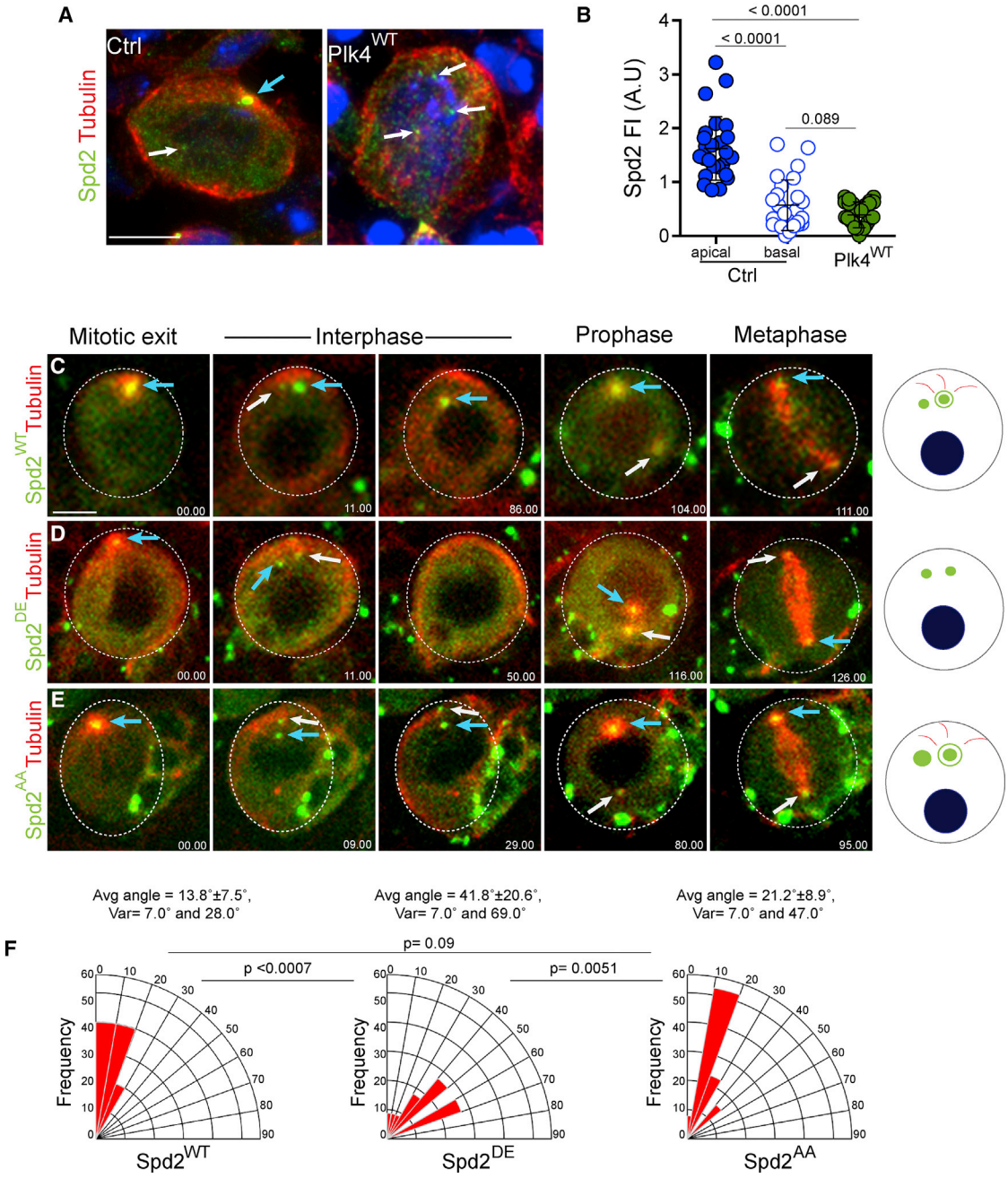

Figure 4. Spd2 Phosphomutant NBs Display Centrosome Asymmetry and MSO Defects

(A) Ctrl and Plk4^{WT} interphase NBs immunostained for tubulin (red) and Spd2 (green). DNA in blue. The blue arrow marks the apical centrosome in Ctrl NBs where Spd2 is detectable. White arrows denote centrosomes with low Spd2 levels. Scale, 4 μm.

(B) Dot plot showing Spd2 fluorescent intensity levels at the centrosome in the indicated genotypes (Ctrl apical, 1.6 ± 0.12; Ctrl basal, 0.6 ± 0.09; Plk4^{WT}, 0.4 ± 0.04). Error bars represent means ± SD from at least 3 independent experiments. SS was assessed by unpaired t test.

(C–E) Images from time-lapse movies of GFP-Spd2^{WT} (C), GFP-Spd2^{DE} (D), and GFP-Spd2^{AA} (E) larval NBs. Tubulin (red). See also Figures S1 and S6. Blue arrows mark the centrosome inherited by the NB at the end of mitosis. In the interphase panels, blue arrows mark the centriole that was localized at the apical cortex (apical centriole in Spd2^{WT}) or the centrosome that was maintained at the apical hemisphere for longer periods of time after disengagement. White arrows mark the non-apical centrioles. (Right) Diagrams illustrate centriole behavior in each genotype after disengagement during early interphase. Time, minutes. Scale, 4 μm.

(F) Quantification of the angle between two consecutive mitosis in Spd2^{WT}, Spd2^{DE}, and Spd2^{AA}. SS was assessed by unpaired t test.

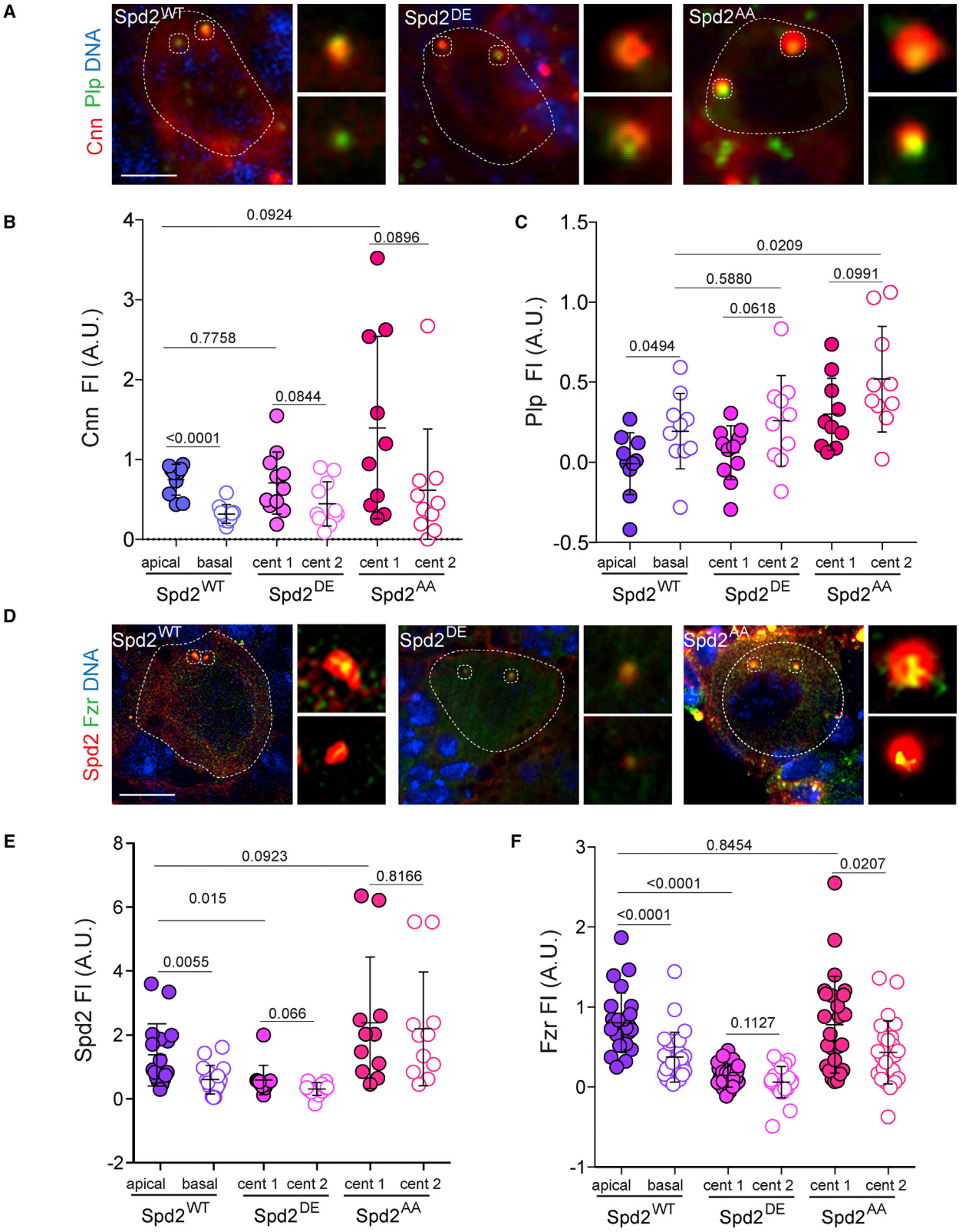

Figure 5. Spd2 Phosphomutants Influence Spd2 and Fzr Centriolar Recruitment without Impacting on Cnn or Plp

(A) Immunostaining of Spd2^{WT}, Spd2^{DE}, and Spd2^{AA} early interphase NBs for Cnn (red) and Plp (green). DNA in blue. Insets show higher magnifications of each centriole. Scale, 4 μm. See also Figures S1 and S6.

(legend continued on next page)

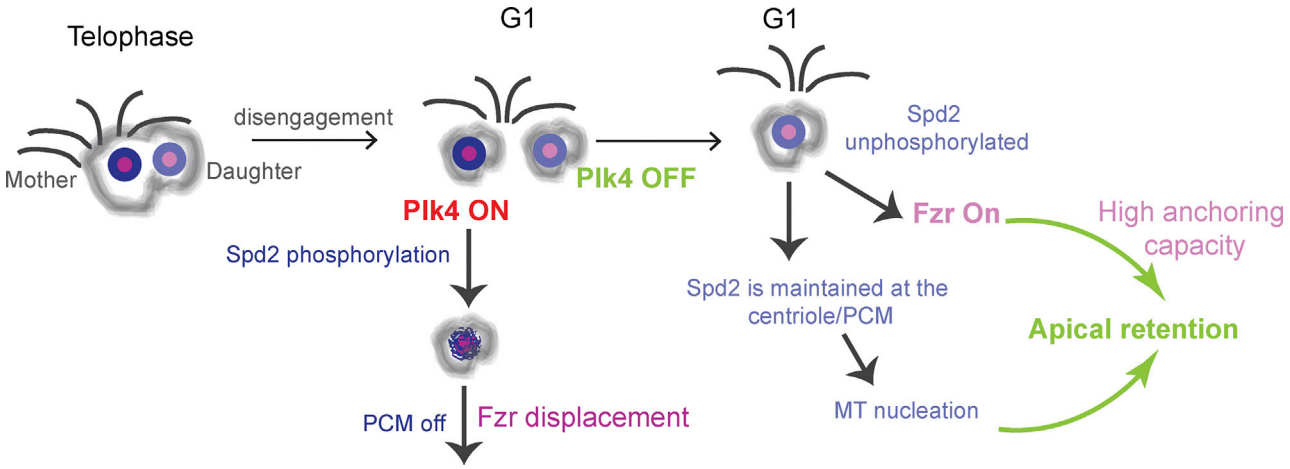

Figure 6. Model of Centriole Symmetry Breaking and Spindle Orientation in *Drosophila* NBs

At the end of mitosis, the mother-daughter centrioles of the NB disengage. The mother (or basal) centriole retains Plk4 activity, which phosphorylates Spd2, causing (1) PCM shedding and, thus, loss of MT nucleation and (2) Fzr displacement, which inhibits apical anchoring. An as yet undiscovered mechanism, Plk4 is inactive on the daughter (or apical) centriole, resulting in the stable maintenance of a centriole-bound population of non-phosphorylated Spd2, which promotes both MT nucleation and Fzr-dependent cortical anchoring.

DISCUSSION

Here, we show that Plk4 plays a new role in the establishment of centrosome asymmetry and MSO in *Drosophila* NSCs. Our findings are consistent with a model where upon centriole disengagement at mitotic exit, the mother centriole inherits Plk4, which triggers centriole movement towards the NB basal side by disrupting microtubule-organizing center (MTOC) activity (Figure 6). Our data suggest that Plk4 needs to be removed or inactivated at the apical centriole, in order to ensure maintenance of MTOC activity. Although the model predicts an unequal distribution of Plk4 between the two NB centrioles, we are unable to test this aspect of the model. Endogenous Plk4 protein levels are extremely low and, despite several attempts to raise antibodies, we were unable to detect endogenous Plk4. Expression of GFP-tagged Plk4 under control of endogenous or weak promoters resulted in the stabilization of the protein, which invariably leads to increased activity and the unwanted supernumerary centrosomes (Basto et al., 2008; Aydogan et al., 2018).

In this model, active centriole-bound Plk4 targets Spd2, triggering Spd2 displacement and promoting, most likely, loss of additional PCM proteins from the basal centriole. It is thus conceivable that mother centrioles lacking Spd2 lose MT nucleation capacity, which induce their movement toward the basal side. It has been previously shown that asymmetric loss of PCM in the basal centriole was sufficient to trigger movement toward the basal side of the NB (Rebollo et al., 2007; Rusan and Peifer, 2007). Further, Spd2 removal also results in the loss of Fzr and consequently disables a previously undescribed second mechanism that contributes to maintaining centrosomes at the apical cortex or hemisphere. It will be important to investigate whether Spd2 mutants, which did not show defects in MSO during mitosis (Dix and Raff, 2007), display altered centriole behavior during interphase.

How Fzr promotes apical anchoring remains to be determined. Our findings support the idea that Fzr promotes centriole apical localization in an APC/C-independent manner. Although we have not identified a mechanism that displaces or inhibits Plk4 on the apical centriole, it is still possible that Fzr promotes apical anchoring by regulating, either directly or indirectly, the levels or activity of Plk4 at the apical centriole. However, we did not detect an interaction between Plk4 and Fzr in *Drosophila* brain extracts (D.G. and R.B., unpublished data). The observation that Fzr is absent from mitotic centrosomes in Ctrl NBs suggests that dynamic centrosome movements (typical of mitosis to allow efficient MT interactions with the cortex and chromosomes) require Fzr removal away from the centrosome. Moreover, the asymmetric maintenance of Fzr at the apical centriole, soon after disengagement, correlates with the low mobility typical of this centrosome. It is thus possible that maintenance of Fzr at the

(B and C) Dot plot showing Cnn and Plp fluorescent intensity levels on centrioles in the indicated genotypes (Cnn– $Spd2^{WT}$: Ctrl apical 0.7 ± 0.06, Ctrl basal 0.3 ± 0.04; $Spd2^{DE}$: Cent1 0.7 ± 0.1, Cent2 0.4 ± 0.08; $Spd2^{AA}$: Cent1 1.4 ± 0.4, Cent2 0.6 ± 0.2 and Plp – $Spd2^{WT}$: Ctrl apical – 0.01 ± 0.06, Ctrl basal 0.2 ± 0.07; $Spd2^{DE}$: Cent1 0.06 ± 0.05, Cent2 0.3 ± 0.09; $Spd2^{AA}$: Cent1 0.3 ± 0.07, Cent2 0.5 ± 0.1). Error bars represent means ± SD from at least 3 independent experiments. SS was assessed by unpaired t test.

(D) Images of $Spd2^{WT}$, $Spd2^{DE}$, and $Spd2^{AA}$ early interphase NBs showing Spd2 (red) and Fzr (green). DNA, blue. Insets show higher magnifications of each centriole. Scale, 4 μm.

(E and F) Dot plot showing Spd2 and Fzr fluorescent intensity levels on centrioles in the indicated genotypes. (Spd2 – $Spd2^{WT}$: Ctrl apical 1.4 ± 0.2, Ctrl basal 0.6 ± 0.1; $Spd2^{DE}$: Cent1 0.6 ± 0.1, Cent2 0.3 ± 0.06; $Spd2^{AA}$: Cent1 2.3 ± 0.6, Cent2 2.1 ± 0.5 and Fzr- $Spd2^{WT}$: Ctrl apical 0.8 ± 0.07, Ctrl basal 0.4 ± 0.06; $Spd2^{DE}$: Cent1 0.1 ± 0.02, Cent2 0.06 ± 0.04; $Spd2^{AA}$: Cent1 0.7 ± 0.1, Cent2 0.4 ± 0.07). Error bars represent means ± SD from at least 3 independent experiments. SS was assessed by unpaired t test.

apical centriole functions as a barrier to mobility. We speculate that such an effect could be direct (Fzr itself can assemble in high-order structures to inhibit centriole mobility) or indirect (through a yet unknown interactor). Importantly, our work shows that maintenance of Spd2 at the apical centriole serves two major functions: PCM retention, MT nucleation and Fzr recruitment to inhibit mobility.

The functions of Plk4 and Spd2 uncovered and described here establish an unexpected association between the centrosome biogenesis machinery (centriole duplication and PCM recruitment) and centrosome asymmetry and spindle positioning apparatus. Additionally, we have identified a mechanism of apical centriole anchoring that appears to compensate for centriole duplication defects in NSCs by promoting apical retention. It will be interesting to investigate whether, the partial loss-of-function mutations in Plk4 described in humans, which cause microcephaly and dwarfism, support centriole retention at the apical cortex of NSCs (Martin et al., 2014; Tsutsumi et al., 2016; Shaheen et al., 2014). This might be beneficial not only by conferring the capacity to assemble primary cilia but also to ensure stem cell viability due to the presence of a centriole (Lambrus and Holland, 2017). Further, it will be important to investigate whether centrosome repositioning described during epithelial mesenchymal transition (EMT) or at mitotic exit (Burute et al., 2017; Piel et al., 2001) also relies on these mechanisms.

STAR★METHODS

Detailed methods are provided in the online version of this paper and include the following:

- KEY RESOURCES TABLE
- CONTACT FOR REAGENT AND RESOURCES SHARING
- EXPERIMENTAL MODEL AND SUBJECT DETAILS
  - Experimental Animals
  - Fly Stocks
  - Cell Lines
- METHOD DETAILS
  - Generation of *Drosophila* Transgenic Lines
  - Generation of Spd2 Fragments
  - Generation of Spd2 Phosphomutant Transgenes for S2 Experiments
  - Expression of Plk4 and Spd2 Transgenes
  - Live Imaging
  - Immunohistochemistry and Antibodies
  - Drug Treatments
  - Western Blot of Spd2 Transgenic Lines
  - *In Vitro* Kinase Assays and Mass Spectrometry
  - RNAi of *Drosophila* S2 Cells
  - Co-Immunoprecipitation and Immunoblotting
  - Synthesis of Spd2 dsRNA
  - Image Acquisition
- QUANTIFICATION AND STATISTICAL ANALYSIS
  - Characterization of Centriole Behavior
  - Stabilization and Tracking Centriole Dynamics in Time-lapse Movies
  - Analysis of Spindle Orientation after Two Consecutive Mitosis
  - Analysis of Spindle Orientation in Mitotic NBs
  - Analysis of Centrosome Position in NBs
  - Characterization of Centrosomal Protein Levels in Interphase Centrioles
  - Statistical Analysis

SUPPLEMENTAL INFORMATION

Supplemental Information can be found online at https://doi.org/10.1016/j.devcel.2019.04.036.

ACKNOWLEDGMENTS

We dedicate this work to the memory of Giuseppe Boccia. We thank J. Raff, Y. Bellaiche, T. Lee, C. Doe, the Bloomington Stock Center, and BestGene for stocks and reagents; L. Sengmanivong, V. Fraisier, and L. Leconte of the NIC at the IC for valuable help with microscopy; P. Maiuri and M. Rujano for help with data analysis; V. Marthiens, D. Vargas, S. Gemble, O. Goudiam, A. Echard, M. Piel, A. Audibert, J. Azimzadeh, M. H. Verlhac, M. Bornens, J. Raff, and C. Gonzalez for discussions and/or critical comments on the manuscript. Financial support from an ERC starting grant CentroStemCancer 242598, a FRM installation and ATIP grants, the Institut Curie and CNRS. G.C.R. is grateful for support from NCI P30CA23074 and NIGMS R01 GM110166 and GM126035. D.G. was supported by PhD fellowships from IC and FRM. The Basto laboratory is a member of the Labex CelTisPhyBio

AUTHOR CONTRIBUTIONS

D.G. and R.B. conceived the project, analyzed the data, and, together with G.C.R., wrote the manuscript. D.G. performed most of the experimental procedures. C.P. generated tools and most of the transgenic fly stocks. J.M.R, D.W.B., and G.C.R. conceived and performed kinase assays, mass spectrometry, and S2 cell experiments. D.G. generated $Plk4^{WT}$ transgenic fly stocks. A.S. helped with the maintenance of fly stocks, crosses, and dissection, and D.-B. and V.R. identified the methodology used to track centrosome or centriole behavior in time-lapse movies and the representation of their dynamics. Y.K. shared unpublished data. A.G. and M.N. helped R.B. to set up the live imaging of some fly strains. R.B. supervised the project.

DECLARATION OF INTERESTS

The authors declare no competing interests.

Received: December 13, 2017
Revised: March 8, 2019
Accepted: April 23, 2019
Published: May 23, 2019

REFERENCES

Adams, J., Behnke, M., Chen, S., Cruickshank, A.A., Dick, L.R., Grenier, L., Klunder, J.M., Ma, Y.T., Plamondon, L., and Stein, R.L. (1998). Potent and selective inhibitors of the proteasome: dipeptidyl boronic acids. Bioorg. Med. Chem. Lett. *8*, 333–338.

Ahmad, K., and Henikoff, S. (2001). Modulation of a transcription factor counteracts heterochromatic gene silencing in Drosophila. Cell *104*, 839–847.

Albertson, R., Chabu, C., Sheehan, A., and Doe, C.Q. (2004). Scribble protein domain mapping reveals a multistep localization mechanism and domains necessary for establishing cortical polarity. J. Cell Sci. *117*, 6061–6070.

Albertson, R., and Doe, C.Q. (2003). Dlg, Scrib and Lgl regulate neuroblast cell size and mitotic spindle asymmetry. Nat. Cell Biol. *5*, 166–170.

Aydogan, M.G., Wainman, A., Saurya, S., Steinacker, T.L., Caballe, A., Novak, Z.A., Baumbach, J., Muschalik, N., and Raff, J.W. (2018). A homeostatic clock sets daughter centriole size in flies. J. Cell Biol. *217*, 1233–1248.

Basto, R., Brunk, K., Vinadogrova, T., Peel, N., Franz, A., Khodjakov, A., and Raff, J.W. (2008). Centrosome amplification can initiate tumorigenesis in flies. Cell *133*, 1032–1042.

Basto, R., Lau, J., Vinogradova, T., Gardiol, A., Woods, C.G., Khodjakov, A., and Raff, J.W. (2006). Flies without centrioles. Cell *125*, 1375–1386.

Bettencourt-Dias, M., Rodrigues-Martins, A., Carpenter, L., Riparbelli, M., Lehmann, L., Gatt, M.K., Carmo, N., Balloux, F., Callaini, G., and Glover, D.M. (2005). SAK/PLK4 is required for centriole duplication and flagella development. Curr. Biol. *15*, 2199–2207.

Blachon, S., Gopalakrishnan, J., Omori, Y., Polyanovsky, A., Church, A., Nicastro, D., Malicki, J., and Avidor-Reiss, T. (2008). Drosophila asterless and vertebrate Cep152 are orthologs essential for centriole duplication. Genetics *180*, 2081–2094.

Brand, A.H., and Perrimon, N. (1993). Targeted gene expression as a means of altering cell fates and generating dominant phenotypes. Development *118*, 401–415.

Brownlee, C.W., Klebba, J.E., Buster, D.W., and Rogers, G.C. (2011). The protein phosphatase 2A regulatory subunit Twins stabilizes Plk4 to induce centriole amplification. J. Cell Biol. *195*, 231–243.

Burute, M., Prioux, M., Blin, G., Truchet, S., Letort, G., Tseng, Q., Bessy, T., Lowell, S., Young, J., Filhol, O., et al. (2017). Polarity reversal by centrosome repositioning primes cell scattering during epithelial-to-mesenchymal transition. Dev. Cell *40*, 168–184.

Castellanos, E., Dominguez, P., and Gonzalez, C. (2008). Centrosome dysfunction in Drosophila neural stem cells causes tumors that are not due to genome instability. Curr. Biol. *18*, 1209–1214.

Caussinus, E., and Gonzalez, C. (2005). Induction of tumor growth by altered stem-cell asymmetric division in Drosophila melanogaster. Nat. Genet. *37*, 1125–1129.

Conduit, P.T., Brunk, K., Dobbelaere, J., Dix, C.I., Lucas, E.P., and Raff, J.W. (2010). Centrioles regulate centrosome size by controlling the rate of Cnn incorporation into the PCM. Curr. Biol. *20*, 2178–2186.

Conduit, P.T., Richens, J.H., Wainman, A., Holder, J., Vicente, C.C., Pratt, M.B., Dix, C.I., Novak, Z.A., Dobbie, I.M., Schermelleh, L., et al. (2014). A molecular mechanism of mitotic centrosome assembly in Drosophila. Elife *3*, e03399.

Conduit, P.T., Wainman, A., and Raff, J.W. (2015). Centrosome function and assembly in animal cells. Nat. Rev. Mol. Cell Biol. *16*, 611–624.

Davis, R. (2003). RE: P{tubP-GAL80ts} construct and insertions. Type to CENTER, B. S.

Dix, C.I., and Raff, J.W. (2007). Drosophila Spd-2 recruits PCM to the sperm centriole, but is dispensable for centriole duplication. Curr. Biol. *17*, 1759–1764.

Dobbelaere, J., Josué, F., Suijkerbuijk, S., Baum, B., Tapon, N., and Raff, J. (2008). A genome-wide RNAi screen to dissect centriole duplication and centrosome maturation in Drosophila. PLoS Biol. *6*, e224.

Farina, F., Gaillard, J., Guérin, C., Couté, Y., Sillibourne, J., Blanchoin, L., and Théry, M. (2016). The centrosome is an actin-organizing centre. Nat. Cell Biol. *18*, 65–75.

Fu, J., and Glover, D.M. (2012). Structured illumination of the interface between centriole and peri-centriolar material. Open Biol. *2*, 120104.

Galletta, B.J., Fagerstrom, C.J., Schoborg, T.A., Mclamarrah, T.A., Ryniawec, J.M., Buster, D.W., Slep, K.C., Rogers, G.C., and Rusan, N.M. (2016). A centrosome interactome provides insight into organelle assembly and reveals a non-duplication role for Plk4. Nat. Commun. *7*, 12476.

Gogendeau, D., Siudeja, K., Gambarotto, D., Pennetier, C., Bardin, A.J., and Basto, R. (2015). Aneuploidy causes premature differentiation of neural and intestinal stem cells. Nat. Commun. *6*, 8894.

Gustafsson, M.G., Shao, L., Carlton, P.M., Wang, C.J., Golubovskaya, I.N., Cande, W.Z., Agard, D.A., and Sedat, J.W. (2008). Three-dimensional resolution doubling in wide-field fluorescence microscopy by structured illumination. Biophys. J. *94*, 4957–4970.

Habedanck, R., Stierhof, Y.D., Wilkinson, C.J., and Nigg, E.A. (2005). The polo kinase Plk4 functions in centriole duplication. Nat. Cell Biol. *7*, 1140–1146.

Homem, C.C., and Knoblich, J.A. (2012). Drosophila neuroblasts: a model for stem cell biology. Development *139*, 4297–4310.

Huang, J.Y., and Raff, J.W. (2002). The dynamic localisation of the Drosophila APC/C: evidence for the existence of multiple complexes that perform distinct functions and are differentially localised. J. Cell Sci. *115*, 2847–2856.

Jacobs, H., Richter, D., Venkatesh, T., and Lehner, C. (2002). Completion of mitosis requires neither fzr/rap nor fzr2, a male germline-specific Drosophila Cdh1 homolog. Curr. Biol. *12*, 1435–1441.

Januschke, J., and Gonzalez, C. (2010). The interphase microtubule aster is a determinant of asymmetric division orientation in Drosophila neuroblasts. J. Cell Biol. *188*, 693–706.

Januschke, J., Llamazares, S., Reina, J., and Gonzalez, C. (2011). Drosophila neuroblasts retain the daughter centrosome. Nat. Commun. *2*, 243.

Januschke, J., Reina, J., Llamazares, S., Bertran, T., Rossi, F., Roig, J., and Gonzalez, C. (2013). Centrobin controls mother-daughter centriole asymmetry in Drosophila neuroblasts. Nat. Cell Biol. *15*, 241–248.

Klebba, J.E., Buster, D.W., Mclamarrah, T.A., Rusan, N.M., and Rogers, G.C. (2015). Autoinhibition and relief mechanism for Polo-like kinase 4. Proc. Natl. Acad. Sci. USA *112*, E657–E666.

Lambrus, B.G., and Holland, A.J. (2017). A new mode of mitotic surveillance. Trends Cell Biol. *27*, 314–321.

Lee, C.Y., Robinson, K.J., and Doe, C.Q. (2006). Lgl, Pins and aPKC regulate neuroblast self-renewal versus differentiation. Nature *439*, 594–598.

Lee, H.S., Simon, J.A., and Lis, J.T. (1988). Structure and expression of ubiquitin genes of Drosophila melanogaster. Mol. Cell. Biol. *8*, 4727–4735.

Lerit, D.A., and Rusan, N.M. (2013). PLP inhibits the activity of interphase centrosomes to ensure their proper segregation in stem cells. J. Cell Biol. *202*, 1013–1022.

Lucas, E.P., and Raff, J.W. (2007). Maintaining the proper connection between the centrioles and the pericentriolar matrix requires Drosophila centrosomin. J. Cell Biol. *178*, 725–732.

Marthiens, V., Rujano, M.A., Pennetier, C., Tessier, S., Paul-Gilloteaux, P., and Basto, R. (2013). Centrosome amplification causes microcephaly. Nat. Cell Biol. *15*, 731–740.

Martin, C.A., Ahmad, I., Klingseisen, A., Hussain, M.S., Bicknell, L.S., Leitch, A., Nürnberg, G., Toliat, M.R., Murray, J.E., Hunt, D., et al. (2014). Mutations in PLK4, encoding a master regulator of centriole biogenesis, cause microcephaly, growth failure and retinopathy. Nat. Genet. *46*, 1283–1292.

Martinez-Campos, M., Basto, R., Baker, J., Kernan, M., and Raff, J.W. (2004). The Drosophila pericentrin-like protein is essential for cilia/flagella function, but appears to be dispensable for mitosis. J. Cell Biol. *165*, 673–683.

Mcguire, S.E., Mao, Z., and Davis, R.L. (2004). Spatiotemporal gene expression targeting with the TARGET and gene-switch systems in Drosophila. Sci. STKE *2004*, pl6.

Meghini, F., Martins, T., Tait, X., Fujimitsu, K., Yamano, H., Glover, D.M., and Kimata, Y. (2016). Targeting of Fzr/Cdh1 for timely activation of the APC/C at the centrosome during mitotic exit. Nat. Commun. *7*, 12607.

Mennella, V., Keszthelyi, B., Mcdonald, K.L., Chhun, B., Kan, F., Rogers, G.C., Huang, B., and Agard, D.A. (2012). Subdiffraction-resolution fluorescence microscopy reveals a domain of the centrosome critical for pericentriolar material organization. Nat. Cell Biol. *14*, 1159–1168.

Moutinho-Pereira, S., Debec, A., and Maiato, H. (2009). Microtubule cytoskeleton remodeling by acentriolar microtubule-organizing centers at the entry and exit from mitosis in Drosophila somatic cells. Mol. Biol. Cell *20*, 2796–2808.

Obino, D., Farina, F., Malbec, O., Sáez, P.J., Maurin, M., Gaillard, J., Dingli, F., Loew, D., Gautreau, A., Yuseff, M.I., et al. (2016). Actin nucleation at the centrosome controls lymphocyte polarity. Nat. Commun. *7*, 10969.

Peel, N., Stevens, N.R., Basto, R., and Raff, J.W. (2007). Overexpressing centriole-replication proteins in vivo induces centriole overduplication and de novo formation. Curr. Biol. *17*, 834–843.

Piel, M., Nordberg, J., Euteneuer, U., and Bornens, M. (2001). Centrosome-dependent exit of cytokinesis in animal cells. Science *291*, 1550–1553.

Ramdas Nair, A., Singh, P., Salvador Garcia, D., Rodriguez-Crespo, D., Egger, B., and Cabernard, C. (2016). The microcephaly-associated protein Wdr62/CG7337 is required to maintain centrosome asymmetry in Drosophila neuroblasts. Cell Rep. *14*, 1100–1113.

Rebollo, E., Sampaio, P., Januschke, J., Llamazares, S., Varmark, H., and González, C. (2007). Functionally unequal centrosomes drive spindle

orientation in asymmetrically dividing Drosophila neural stem cells. Dev. Cell *12*, 467–474.

Riparbelli, M.G., and Callaini, G. (2011). Male gametogenesis without centrioles. Dev. Biol. *349*, 427–439.

Rusan, N.M., and Peifer, M. (2007). A role for a novel centrosome cycle in asymmetric cell division. J. Cell Biol. *177*, 13–20.

San-Juán, B.P., and Baonza, A. (2011). The bHLH factor deadpan is a direct target of Notch signaling and regulates neuroblast self-renewal in Drosophila. Dev. Biol. *352*, 70–82.

Schindelin, J., Arganda-Carreras, I., Frise, E., Kaynig, V., Longair, M., Pietzsch, T., Preibisch, S., Rueden, C., Saalfeld, S., Schmid, B., et al. (2012). Fiji: an open-source platform for biological-image analysis. Nat. Methods *9*, 676–682.

Shaheen, R., Al Tala, S., Almoisheer, A., and Alkuraya, F.S. (2014). Mutation in PLK4, encoding a master regulator of centriole formation, defines a novel locus for primordial dwarfism. J. Med. Genet. *51*, 814–816.

Singh, P., Ramdas Nair, A., and Cabernard, C. (2014). The centriolar protein Bld10/Cep135 is required to establish centrosome asymmetry in Drosophila neuroblasts. Curr. Biol. *24*, 1548–1555.

Sivakumar, S., and Gorbsky, G.J. (2015). Spatiotemporal regulation of the anaphase-promoting complex in mitosis. Nat. Rev. Mol. Cell Biol. *16*, 82–94.

Stevens, N.R., Raposo, A.A., Basto, R., St Johnston, D., and Raff, J.W. (2007). From stem cell to embryo without centrioles. Curr. Biol. *17*, 1498–1503.

Tsutsumi, M., Yokoi, S., Miya, F., Miyata, M., Kato, M., Okamoto, N., Tsunoda, T., Yamasaki, M., Kanemura, Y., Kosaki, K., et al. (2016). Novel compound heterozygous variants in PLK4 identified in a patient with autosomal recessive microcephaly and chorioretinopathy. Eur. J. Hum. Genet. *24*, 1702–1706.

Zhang, Y., Malone, J.H., Powell, S.K., Periwal, V., Spana, E., Macalpine, D.M., and Oliver, B. (2010). Expression in aneuploid Drosophila S2 cells. PLoS Biol. *8*, e1000320.

Zhu, S., Lin, S., Kao, C.F., Awasaki, T., Chiang, A.S., and Lee, T. (2006). Gradients of the Drosophila Chinmo BTB-zinc finger protein govern neuronal temporal identity. Cell *127*, 409–422.

STAR★METHODS

KEY RESOURCES TABLE

REAGENT or RESOURCE	SOURCE	IDENTIFIER
Antibodies		
Rabbit polyclonal anti-Spd2	(Dix and Raff, 2007)	RRID: AB_2567456
Rabbit polyclonal anti-Plp	(Martinez-Campos et al., 2004)	N/A
Rabbit polyclonal anti-aPKC	Santa Cruz	Cat# SC116
Guinea pig polyclonal anti-Spd2	This paper	N/A
Guinea pig polyclonal anti-Cnn	(Lucas and Raff, 2007)	N/A
Mouse monoclonal anti-α-Tubulin (clone DM1A), purified antibody	Sigma-Aldrich	Cat# T6199; RRID: AB_477583
Mouse monoclonal anti-α-Tubulin (clone DM1A), ascites fluid	Sigma-Aldrich	Cat# T9026; RRID: AB_477593
Mouse monoclonal anti-prospero	DSHB	MR1A; RRID: AB_528440
RFP-Booster (Atto 594)	Chromotek	Cat# rba594; RRID: AB_2631390
Mouse anti-GFP (clone JL-8)	Clonetech Laboratories	Cat# 632381; RRID: AB_2313808
Mouse anti-HA (clone HA-7)	Sigma-Aldrich	Cat# H3663; RRID: AB_262051
Mouse anti-V5	Invitrogen	Cat# 46-0705; RRID: AB_2556564
Alexa-Fluor 488 goat anti-rabbit	Thermo Fisher Scientific	A11008
Alexa-Fluor 546 goat anti-mouse	Thermo Fisher Scientific	A11031
Alexa-Fluor 633 goat anti-guinea pig	Thermo Fisher Scientific	A21105
Fluorescent molecules		
546-conjugated Phalloidin	Thermo Fisher Scientific	A22283
647-conjugated Phalloidin	Thermo Fisher Scientific	A22287
ATTO 488-Booster	ChromoTek	AD 488-21
ATTO 594-Booster	ChromoTek	AD 594-21
Bacterial and Virus Strains		
DH5α™ Competent Cells	Thermo Fisher Scientific	Cat# 18258012
One Shot™ BL21DE3 Competent Cells	Thermo Fisher Scientific	Cat# C600003
Chemicals, Peptides, and Recombinant Proteins		
Demecolcine	Sigma-Aldrich	Cat# D7385; CAS: 477-30-5
Cytochalasin D	Sigma-Aldrich	C8273
Bortezomib (PS-341)	Selleck Chemicals	Cat# S1013; CAS: 179324-69-7
Pfu Ultra HF DNA polymerase	Agilent Technologies Genomics	Cat# 600380
Schneider's *Drosophila* medium	Gibco	Cat# 21720-024
Sf-900 II serum free medium	ThermoFisher	Cat# 10902096
Nucleofector II	Amaxa (Lonza)	Cat# AAD-1001S
Fetal bovine serum	Gibco	Cat# 10500
Penicillin–streptomycin	Gibco	Cat# 15140
Acetic acid	VWR	Cat# 20103 295
Protein-A conjugated Dynabeads	Invitrogen	Cat# 10001 D
Dimethyl pimelimidate dihydrochloride	Sigma-Aldrich	Cat# D8388
Sodium azide (NaN_3)	Fisher	Cat# S227I
Dithiothreitol (DTT)	Fisher	Cat# BP172
Phenylmethylsophonyl fluoride (PMSF)	Sigma-Aldrich	Cat# 78830
Soybean trypsin inhibitor, type II-S (SBTI)	Sigma-Aldrich	Cat# T9128
SIGMAFAST protease inhibitor cocktail, EDTA-free	Sigma-Aldrich	Cat# S8830

(*Continued on next page*)

Continued

REAGENT or RESOURCE	SOURCE	IDENTIFIER
MBP-Spd2-NT1 (a.a. 1-84)	This paper	N/A
GST-Spd2-NT2 (a.a. 85-340)	This paper	N/A
GST-Spd2-M (a.a. 341-662)	This paper	N/A
GST-Spd2-C (a.a. 663-1146)	This paper	N/A
Plk4(a.a.1-317)-FLAG-His_6	(Brownlee et al., 2011)	N/A
Experimental Models: Organisms/Strains		
D. melanogaster: UAS-GFP-Plk4^{KD} (Plk4^{KD})	This paper	N/A
D. melanogaster: UAS-GFP-Plk4^{WT} (Plk4^{WT})	This paper	N/A
D. melanogaster: Ubq-RFP-Fzr	This paper	N/A
D. melanogaster: Ubq-α-Tubulin-RFP	(Dobbelaere et al., 2008)	N/A
D. melanogaster: Ubq-α-Tubulin-GFP	(Dobbelaere et al., 2008)	N/A
D. melanogaster: Ubq-RFP-Sas-6	(Peel et al., 2007)	N/A
D. melanogaster: UAS-Spd2WT	This paper	N/A
D. melanogaster: UAS-Spd2DE	This paper	N/A
D. melanogaster: UAS-Spd2AA	This paper	N/A
D. melanogaster: Sas-4^{s2214}	(Basto et al., 2006)	BDSC# 12119; FBst# 0012119
D. melanogaster: Fzr^{rapG0418}	(Jacobs et al., 2002)	BDSC# 12297 FBst# 0012297
D. melanogaster: Ubq-GFP-Cdc27	(Huang and Raff, 2002)	N/A
D. melanogaster: WorGAL4	(Lee et al., 2006)	N/A
D. melanogaster: AseGAL4	(Zhu et al., 2006)	N/A
D. melanogaster: ActGAL4	Bloomington Drosophila Stock Center (Ahmad and Henikoff, 2001)	BDSC# 25374 FBti# 0127834
D. melanogaster: GAL80^{ts}	Bloomington Drosophila Stock Center (Davis, 2003	BDSC# 7108
D. melanogaster: Sak^{c06612} (Plk4^{Mut})	(Bettencourt-Dias et al., 2005)	BDSC# 17774 FBst# 0017774
D. melanogaster: wf	(Basto et al., 2006)	
D. melanogaster: y^1w^{1118};PBac{y^+-attp-9A}VK00020	Bloomington Drosophila Stock Center	BDSC# 9738 FBti# 0076441
Cell lines		
Drosophila S2 cells	Invitrogen (Zhang et al., 2010)	Cat# R69007
Oligonucleotides		
Plk4^{KD} construct generation: F 5'- GTCAAGATAG CCAACTTTGGACTGGCC-3' and R 5'- GGCCAGT CCAAAGTTGGCTATCTTGAC-3'	This paper	N/A
Ubq-RFP-Fzr construct generation: F 5'-GGGGAC AAGTTTGTACAAAAAAGCAGGCTTC ATGTTTAGTCCCGAGTACGAGAAG-3' and R 5'-GGGGACCACTTTGTACAA GAAAGCTGGGT CTTATCTGATATTGGCAAACAGATT-3'	This paper	N/A
UAS-RFP-Spd2 constructs generation: F 5'- cgcgcg ACTAGTGGCGGCACCGGCGGCACC ATGGACAGTAGCAGTGGAAGCCAA-3' and R 5'-cgc gcgCCGCGGTTAAAACTAATCGGGAC-3'	This paper	N/A
RFP cloning from pURW: F 5'- cgcgcgGATATC ATGGCCTCCTCCGAGGACGTCATC-3' and R: 5'- cgcgcgGGATCCGGCGCCGGTGGAGTGG CGGCCCTC-3'	This paper	N/A

(*Continued on next page*)

Continued

REAGENT or RESOURCE	SOURCE	IDENTIFIER
MBP-Spd2-NT1 constructs generation: F 5'-gcgcgc GGATCCATGGACAGTAGCAGTGGAAGCCAA-3' and R 5'- gcgcgcAAGCTTTTACTGGAGGGCAGTG CTCTTTGCTTG – 3'	This paper	N/A
GST-Spd2-NT2 constructs generation: F 5'-cgcgcg GGATCCATGCGCTTGTCCACAAACATCTCG – 3' and R 5' – cgcgcgCTCGAGTTATGGCTGTGGGGTC TTCTCGCCAAC – 3'	This paper	N/A
GST-Spd2-M constructs generation: F 5' -cgcgcg GGATCCGACAATAAAACATACACTAAAACG-3' and R 5'- cgcgcgCTCGAGTTATGTGAATCCGCT GGTGGAACTGGC - 3'	This paper	N/A
GST-Spd2-C constructs generation: F 5' - gcgcgc GGATCCGCGAGTGGAAGACGTGGGTTGGGA - 3' and R 5' - cgcgcgCTCGAGTTAAAATTTAAAACTAA TCGGGACACT - 3'	This paper	N/A
GFP-Spd2 constructs generation: F 5' – cgcgGGTA CC**T**ATGGTGAGCAAGGGCAGGAG – 3' and 5' – cgcg ACTAGTCTTGTACAGCTCGTCCATGCC – 3'	This paper	N/A
Spd2-UTR dsRNA synthesis: F 5' – TAATACGACTCA CTATAGGGGTTTTCGCGTTCGCACTGCAAACTGTA ACTGTTTAAGGACAAAGCGGATTTGTTTTATTTGTG CCTGC – 3' and R 5' – TAATACGACTCACTATAGGG CTTTTAGGAAACAAGCG – 3'	This paper	N/A
V5-Spd2 constructs generation: F 5' - GGGGGGATC TAGATCGGGGTACCATGggtaagcctatccctaaccctctcc tcggtctcgattctacgATGGACAGTAGCAGTGGAAGCC – 3' and R 5' – GGCTTCCACTGCTACTGTCCATcgtagaatcg agaccgaggagagggttagggataggcttaccCATGGTACCCCG ATCTAGATCCCCCC – 3'	This paper	N/A
V5-Cnn construct from EST: F 5' – GGGGATCTAGATCG GGGTACCATGggtaagcctatccctaaccctctcctcggtctcgattc tacgATGGACCAGTCTAAA – 3' and R 5' – CGCCACTGTG CTGGATATCTTATAACTCATTCTCCATGTTTGAGCGAAC – 3'	This paper	N/A
Recombinant DNA		
attB-P[acman]-Ap^{r} plasmid	DGRC	GenBank EF106980
attB-pUAST-GFP-Plk4^{WT}-SV40	This paper	N/A
attB-pUAST-GFP-Plk4^{KD}-SV40	This paper	N/A
attB-pUAST-GFP-Plk4^{PACT}-SV40	This paper	N/A
pET28a-Plk4(a.a.1-317)-FLAG-His$_6$	(Brownlee et al., 2011)	N/A
pMal-C2X	Addgene	Cat# 75286
pGEX-6P-2	Addgene	Cat# 27-4598-01
pMal-C2X-Spd2-NT1 (a.a. 1-84)	This paper	N/A
pGEX-6P-2-Spd2-NT2 (a.a. 85-340)	This paper	N/A
pGEX-6P-2-Spd2-M (a.a. 341-662)	This paper	N/A
pGEX-6P-2-Spd2-C (a.a. 663-1146)	This paper	N/A
pUbq-RFPNT	(Basto et al., 2008)	N/A
pUbq-RFPNT-Fzr	This paper	N/A
attB-pUAST-RFP-Spd2^{WT}-Sv40	This paper	N/A
attB-pUAST-RFP-Spd2^{DE}-Sv40	This paper	N/A
attB-pUAST-RFP-Spd2^{AA}-Sv40	This paper	N/A
pOT2 Spd2 EST (Clone ID LD24702, DGC EST Library 1.0)	DGRC	CG17286
pMT/V5 His B	ThermoFisher	Cat# V412020
pEGFP C1	Addgene	Catalog #6084-1

(*Continued on next page*)

Continued

REAGENT or RESOURCE	SOURCE	IDENTIFIER
pMT/V5 His B GFP-Spd2^{WT}	This paper	N/A
pMT/V5 His B GFP-Spd2^{AA}	This paper	N/A
pMT/V5 His B GFP-Spd2^{DE}	This paper	N/A
pMT/V5 His C GFP	(Klebba et al., 2015)	N/A
pMT/V5 His B V5-Spd2^{WT}	This paper	N/A
pMT/V5 His B V5-Spd2^{AA}	This paper	N/A
pMT/V5 His B V5-Spd2^{DE}	This paper	N/A
pOT2 Cnn EST (Clone ID LD19135, DGC EST Library 1.0)	DGRC	CG4832
pMT/V5 His C V5-Cnn	This paper	N/A
pMT/V5 His C Asl V5	(Klebba et al., 2015)	N/A
Software and Algorithms		
Metamorph software 7.7	Molecular devices	N/A
Fiji	(Schindelin et al., 2012)	https://fiji.sc/
Photoshop	Adobe	N/A
GraphPad Prism 7	GraphPad Software, Inc.	N/A
Other		
Glass-bottom 35 mm dish uncoated	MatTek Corporation	P35G-1.5-14-C
Membrane kit, Standard	YSI	SKU098094
Voltalef oil 10S	VWR BDH Prolabo	Cat# 24627.188; CAS: 9002-83-9

CONTACT FOR REAGENT AND RESOURCES SHARING

Further information and requests for resources and reagents should be directed to and will be fulfilled by the Lead Contact, Dr. Renata Basto (renata.basto@curie.fr).

EXPERIMENTAL MODEL AND SUBJECT DETAILS

Experimental Animals

Species: *Drosophila melanogaster*. Flies were raised on *Drosophila* culture medium (0,75% agar, 3,5% cornmeal, 5% yeast, 5,5% sugar, 2,5% methyl, 1% penicillin–streptomycin, 0,4% propionic acid). Flies stocks were maintained at 18°C in plastic vials or plastic bottles. Crosses were maintained at 25°C in plastic vials. Brains were collected from 3rd instar larvae (which were staged as the number of days after egg laying and confirmed with developmental landmarks such as size, mouth hook and position within the tube). For all experiments except *Fzr*^{rapG0418} (Fzr^{mut}) and in combination with Plk4^{KD}, we analyzed male and female since we did not notice any difference between the two sexes. In the case of Fzr^{mut}, we analysed only males. In all experiments, Plk4^{KD}, Plk4^{WT} and Plk4^{PACT} were recombined with the Plk4 mutant-*Sak*^{c06612} (Bettencourt-Dias et al., 2005) (BDSC#17774). Controls (Ctrl) were used accordingly to the experiments (please see Key Resources Table and below for detailed analysis).

Fly Stocks

UAS lines: UAS-GFP-Plk4^{KD} (Plk4^{KD}, this study), UAS-GFP-Plk4^{WT} (Plk4^{WT}, this study).

Reporter lines: Ubq-α-Tubulin-RFP and Ubq-α-Tubulin-GFP (Dobbelaere et al., 2008), Ubq-RFP-Sas-6 (Peel et al., 2007), Ubq-RFP-Fzr (this study), Ubq-GFP-Cdc27 (Huang and Raff, 2002).

Mutant alleles: *Sak*^{c06612} (BDSC#17774, (Bettencourt-Dias et al., 2005)), *Sas-4*^{s2214} (BDSC#12119, (Basto et al., 2006)), Fzr^{rapG0418} (BDSC#12297, (Jacobs et al., 2002)).

Driver lines: WorGAL4 (provided by C. Doe, (Albertson et al., 2004) , AseGAL4 (provided by T. Lee, (Zhu et al., 2006), ActGAL4 (BDSC#25374), GAL80ts (BDSC#7108).*wf* was used as a control strain.

Cell Lines

Female *Drosophila* S2 cells (Zhang et al., 2010) (Invitrogen) were cultured in Sf-900 II (Life Technologies) + Pen/Strep (Gibco) and split every 3-4 days.

METHOD DETAILS

Generation of *Drosophila* Transgenic Lines

The Plk4^{WT} transgene was synthetized by GenScript (GenScript®, NJ, USA) in the pUC57 plasmid, using the coding DNA sequence (CDS) of *Drosophila* Plk4. The Plk4^{KD} allele was generated by site-directed mutagenesis (*Pfu Ultra* HF DNA polymerase, 600380, Agilent Technologies Genomics) from the Plk4^{WT} allele with primers F (5'- GTCAAGATAGCCAACTTTGGACTGGCC-3) and R (5'- GGCCAGTCCAAAGTTGGCTATCTTGAC-3'). Underlined is the triplet coding for D156, mutated into N. All Plk4 versions were initially cloned into a pDONR^{TM}/Zeo plasmid (Invitrogen, CA, USA) to have the GFP at their N-terminus, spaced by a linker of six triplets (GGCGGCACCGGCGGCACC), under the control of the UAS (X5) promoter. At the 3' end, the SV40 sequence was also included (Figure S1). All constructs were validated through Sanger sequencing of the entire coding region. The UAS promoter was combined with the SV40 polyA sequence (ttaattgtttattgcagcttataatggttacaaataaagcaatagcatcacaaatttcacaaataaagcatttttttcactgcattctagttgtggtttgtccaaactcatcaatgtatcttatcagcggccgc), which allows for high expression and stabilization of the Plk4 sequences. To generate all Plk4 transgenic stocks, the PhiC31 integrase-mediated transgenesis system was used. The different Plk4 constructs, flanked by NotI and AscI, were cloned into a P[acman] plasmid containing the *attB* site (DGRC, GeNBank EF106980) and injections were performed by BestGene (BestGene Inc, CA, USA). The Bloomington stock BI9738 (y^1w^{1118};PBac {y^+-attp-9A}VK00020) was used as *attP*-containing docking site strain. All transgenes were inserted in the third chromosome in the insertion site 99F8.

To generate the Ubq-RFP-Fzr stock, the genomic sequence of Fzr was first amplified by PCR with primers F: (5'-GGGGACA AGTTTGTACAAAAAAGCAGGCTTC ATGTTTAGTCCCGAGTACGAGAAG-3') and R: (5'-GGGGACCACTTTGTACAA GAAAGC TGGGTCTTATCTGATATTGGCAAACAGATT-3'). Fzr specific sequences are underlined. The PCR product was then recombined using BP Gateway reaction (Gateway® Technology, Invitrogen, ThermoScientific) into pDONR^{TM}/Zeo plasmid. After sequence validation through Sanger sequencing, Fzr was recombined, using LR Gateway reaction in the pUbq-RFPNT vector (Basto et al., 2008), which allows for moderate expression of the tagged protein (Lee et al., 1988). BestGene performed injections in the w1118 stock. With this system the transgene insertion occurred randomly. For all experiments, stocks with transgenes inserted in the second chromosome were used.

For UAS- RFP-Spd2 stocks, the Spd2 cDNA was cloned in phase with RFP on its N-terminus with the primers F: (5'- cgcgcgACT AGTGGCGGCACCGGCGGCACC ATGGACAGTAGCAGTGGAAGCCAA) and R: (5'-cgcgcgCCGCGGTTAAAACTAATCGGGAC) and SV40 (sequence described above) at its C-terminus with the enzymes Spe1 and SacII in the Bluescript vector. RFP was cloned from the pURW vector (DGRC #1282) with primers F: (5'- cgcgcgGATATCATGGCCTCCTCCGAGGACGTCATC-3') and R: (5'-cgcgcgGGATCCGGCGCCGGTGGAGTGGCGGCCCTC-3') in the Bluescript vector with the enzymes EcoRV and BamHI, spaced by a linker composed of GGTGGT. Spd2 and RFP specific sequences are underlined. Restriction enzymes are in Italic. Spd2DE and Spd2AA constructs were synthetized by GeneART (ThermoFisher). In Spd2DE construct, all serines (Ser) and threonines (Thr) identified were mutated to aspartate (D) with the exception of Thr371, Thr384, Thr458, Thr493, Thr706, Thr754, which were mutated to Glutamate (E). In Spd2AA construct all 28 phosphoresidues identified were mutated to alanines (A). After fusion to RFP and SV40 and sequence validation through Sanger sequencing, all constructs comprising RFP-Spd2-SV40 was subsequently cloned in the P[acman] plasmid using AscI and Not1. Insertion site and transgenesis were performed as mentioned above for Plk4 constructs by BestGene Inc, CA, USA.

Generation of Spd2 Fragments

Spd2 fragments were amplified by PCR from the Spd2 cDNA, using the following primers: for Spd2-NT1 (a.a. 1-84) F 5' - gcgc gcGGATCCATGGACAGTAGCAGTGGAAGCCAA - 3' and R 5' -gcgcgcAAGCTTTTACTGGAGGGCAGTGCTCTTTGCTTG - 3', for Spd2-NT2 (a.a. 85-340) F 5' - cgcgcgGGATCCATGCGCTTGTCCACAAACATCTCG – 3' and R 5' – cgcgcgCTCGAGTTA TGGCTGTGGGGTCTTCTCGCCAAC–3', for Spd2-M (a.a. 341-663) F 5' – cgcgcgGGATCCGACAATAAAACATACACTAAAACG - 3' and R 5' - cgcgcgCTCGAGTTATGTGAATCCGCTGGTGGAACTGGC - 3' and for Spd2-C (a.a. 664–1146) F 5' - gcgcgcGGATCCGCG AGTGGAAGACGTGGGTTGGGA - 3' and R 5' - cgcgcgCTCGAGTTAAAATTTAAAACTAATCGGGACACT - 3'. Spd2 specific sequences are underlined. Restriction enzymes are in Italic. Spd2-NT1 was cloned into the pMal-C2X vector with the enzymes BamHI and HindIII, with MBP on its N-terminus. Spd2-NT2, Spd2-M and Spd2-C were cloned into the pGEX-6P-2 vector with the enzymes BamHI and XhoI, with GST on their N-terminus. After sequence validation through Sanger sequencing, Spd2 fragments were used for *in vitro* kinase assay.

Generation of Spd2 Phosphomutant Transgenes for S2 Experiments

Generation of the GFP-Spd2 phosphomutant transgenes was obtained as follows. GFP was amplified by PCR from the pEGFP C1 vector, flanked with KpnI and SpeI restriction sites, using the following primers: F 5' – cgcgGGTACC**T**ATGGTGAGCAAGGGCAGGAG – 3' and 5' – cgcgACTAGTCTTGTACAGCTCGTCCATGCC – 3'. GFP specific sequences are underlined. Restriction enzymes are in Italic. In the F primer, one T was added between the KpnI site and GFP sequence to maintain the frame in the pMT/V5 HisB vector. Next, Spd2 phosphomutant sequences were recovered from the Bluescript vector (already used for the generation of RFP-Spd2 stocks, see above) by digestion with the enzymes SpeI and SacII and cloned into the pMT/V5 HisB vector with GFP on their N-terminus.

The V5-Spd2 phosphomutants were generated from the GFP-Spd2 phosphomutant (in the pMT/V5 HisB vector) by a megaprimer PCR strategy. GFP sequence was replaced with V5 sequence using the megaprimers F 5' – GGGGGGATCTAGAT CGGGGTACCATGggtaagcctatccctaaccctctcctcggtctcgattctacgATGGACAGTAGCAGTGGAAGCC - 3' and R 5' – GGCTTCC ACTGCTACTGTCCATcgtagaatcgagaccgaggagagggttagggataggcttaccCATGGTACCCCGATCTAGATCCCCCC - 3'. The V5-tag is in lower case and Spd2 specific sequences are underlined. The V5-Spd2 sequences were verified by sequencing. The V5-Cnn construct was PCR amplified from a Cnn EST (Clone ID LD19135, DGC EST Library 1.0) using primers F 5' – GGGGATCTAGA TCGGGGTACCATGggtaagcctatccctaaccctctcctcggtctcgattctacgATGGACCAGTCTAAA - 3' and F 5' – CGCCACTGTGCTGGATATC TTATAACTCATTCTCCATGTTTGAGCGAAC - 3' and then inserted into the pMT/V5 HisC vector. The V5-tag is in lower case and Cnn specific sequences are underlined. Insert sequences were verified by sequencing.

Expression of Plk4 and Spd2 Transgenes

Expression of UAS-transgenes was carried out using either the UAS/GAL4 system (Brand and Perrimon, 1993) or the temporal and regional gene expression targeting (TARGET) method (McGuire et al., 2004). Worniu (Wor)GAL4 (Albertson et al., 2004) and Asense (Ase) GAL4 (Zhu et al., 2006) were used to induce transgene expression exclusively in NBs to perform live imaging experiments. WorGal4 and AseGal4 were recombined with either Ubq-α-Tubulin-RFP or Ubq-α-Tubulin-GFP transgenes (Dobbelaere et al., 2008), localized on the 2nd chromosome. As control for live imaging experiments, to analyze centriole behavior we used the Ubq-Sas-6 RFP line, which was crossed with Ubq-α-Tubulin-GFP,WorG4 or Ubq-α-Tubulin-GFP,AseGal4. As control for live imaging experiments, to analyze centriole behavior we used the Ubq-Sas-6 RFP line was crossed with Ubq-α-Tubulin-GFP, or Ubq-α-Tubulin-GFP, WorG4 or Ubq-α-Tubulin-GFP,AseGal4. All these lines showed similar centriole behavior and cell cycle timings. We referred to them as Ctrls in the text. A recombinant comprising the ActGAL4 (BDSC#25374) and GAL80^{ts} (BDSC#7108) on the 2nd chromosome was used to induce the expression of the transgenes in a temporal manner to be used in immunostaining experiments. At 18C, GAL80^{ts} binds to and inhibits the transcriptional activation domain of GAL4. The fly crosses were established and allowed for larvae to develop at either 18C–20C . Second instar larvae were then moved to 29C in order to inhibit the binding between GAL80^{ts} and GAL4. This leads to the expression of the UAS-transgene within 16-18 hours. Two days after, mid third instar larval brains were dissected for immunostaining. Ctrls were performed with this stock, where the ActGal4Gal80^{ts} recombinants were allowed to develop between 18C-20C, before being placed in the 29C incubator.

Drosophila genotypes and crosses

Figure 1

Control: GFP-Tub, AseGal4/Cyo-GFP; X Ubq RFP-Sas6

Plk4KD: RFP-Tub, AseGal4/Cyo-GFP; Plk4mut /TM6 Tb X +/Cyo-GFP; GFP- Plk4KD, Plk4 mut/ TM6 Tb

Plk4WT: RFP-Tub, AseGal4/Cyo-GFP; Plk4mut /TM6 Tb X +/Cyo-GFP; GFP- Plk4WT, Plk4 mut/ TM6 Tb

Crosses were maintained at 25°C

Figure 2

Control: ActGal4, Gal80ts, /Cyo-GFP; Plk4mut /TM6 Tb

Plk4KD: ActGal4, Gal80ts, /Cyo-GFP; Plk4mut /TM6 Tb X +/Cyo-GFP; GFP- Plk4KD, Plk4 mut/ TM6 Tb

Plk4mut: ActGal4, Gal80ts, /Cyo-GFP; Plk4mut /TM6 Tb

Plk4WT: ActGal4, Gal80ts, /Cyo-GFP; Plk4mut /TM6 Tb X +/Cyo-GFP; GFP- Plk4WT, Plk4 mut/ TM6 Tb

Crosses were maintained at 18 °C for 4 days after egg laying and transferred to 29°C for 48 hrs.

Control: GFP-Tub, AseGal4/Cyo-GFP; X Ubq RFP-Sas6

Plk4KD: RFP-Tub, AseGal4/Cyo-GFP; Plk4mut /TM6 Tb X +/Cyo-GFP; GFP- Plk4KD, Plk4 mut/ TM6 Tb

Crosses were maintained at 25°C

Figure 3

Control: ActGal4, Gal80ts, /Cyo-GFP; Plk4mut /TM6 Tb

Plk4KD: ActGal4, Gal80ts, /Cyo-GFP; Plk4mut /TM6 Tb X +/Cyo-GFP; GFP- Plk4KD, Plk4 mut/ TM6 Tb

Plk4WT: ActGal4, Gal80ts, /Cyo-GFP; Plk4mut /TM6 Tb X +/Cyo-GFP; GFP- Plk4WT, Plk4 mut/ TM6 Tb

Crosses were maintained at 18 °C for 4 days after egg laying and transferred to 29°C for 48hrs.

Fzrmut: Fzr/Fm7 Kr-GFP; If/Cyo-GFP X GFP-Tub/Cyo-GFP

Fzrmut, Plk4KD: Fzr/Fm7 Kr-GFP; GFP- Plk4KD, Plk4 mut/ TM6 Tb X RFP-Tub, AseGal4/Cyo-GFP; Plk4mut /TM6 Tb

Crosses were maintained at 25°C

Fzrmut: Fzr/Fm7 Kr-GFP; If/Cyo-GFP

Fzrmut, Plk4KD: Fzr/Fm7 Kr-GFP; GFP- Plk4KD, Plk4 mut/ TM6 Tb X ActGal4, Gal80ts, /Cyo-GFP; Plk4mut /TM6 Tb

Crosses were maintained at 18 °C for 4 days after egg laying and transferred to 29°C for 48hrs.

Figure 4

Control: wf

Plk4WT: ActGal4, Gal80ts, /Cyo-GFP; Plk4mut /TM6 Tb X +/Cyo-GFP; GFP- Plk4WT, Plk4 mut/ TM6 Tb

Crosses were maintained at 18 °C for 4 days after egg laying and transferred to 29°C for 48hrs.

Spd2WT: If/Cyo-GFP; Spd2WT/TM6Tb X GFP-Tub, AseGal4/Cyo-GFP; Plk4^{mut} /TM6 Tb

Spd2DE: If/Cyo-GFP; Spd2DE/TM6Tb X GFP-Tub, AseGal4/Cyo-GFP; Plk4^{mut} /TM6 Tb

Spd2AA: If/Cyo-GFP; Spd2DE/TM6Tb X GFP-Tub, AseGal4/Cyo-GFP; Plk4^{mut} /TM6 Tb

Crosses were maintained at 25°C
Figure 5
Spd2WT: If/Cyo-GFP; Spd2WT/TM6Tb X ActGal4, Gal80ts/Cyo-GFP; Sb/TM6Tb
Spd2DE: If/Cyo-GFP; Spd2DE/TM6Tb X ActGal4, Gal80ts /Cyo-GFP; Sb/TM6Tb
Spd2AA: If/Cyo-GFP; Spd2DE/TM6Tb X ActGal4, Gal80ts /Cyo-GFP; Sb/TM6Tb
Crosses were maintained at 18 °C for 4 days after egg laying and transferred to 29°C for 48hrs.
SFigure 2
Control: ActGal4, Gal80ts, /Cyo-GFP
Plk4KD: ActGal4, Gal80ts, /Cyo-GFP; Plk4mut /TM6 Tb X +/Cyo-GFP; GFP- Plk4KD, Plk4 mut/ TM6 Tb
Plk4mut: ActGal4, Gal80ts, /Cyo-GFP; Plk4mut /TM6 Tb
Plk4WT: ActGal4, Gal80ts, /Cyo-GFP; Plk4mut /TM6 Tb X +/Cyo-GFP; GFP- Plk4WT, Plk4 mut/ TM6 Tb
Crosses were maintained at 18 °C for 4 days after egg laying and transferred to 29°C for 48hrs.
Plk4mut/TM6Tb
Sas-4mut/TM6Tb
Fzrmut/FM7 Kr-GFP
Ubq-RFP-Sas-6/Cyo-GFP; Sas-4mut/TM6Tb X Ubq-GFP-Tub/Cyo-GFP; Sas-4mut/TM6Tb
Crosses were maintained at 25°C
SFigure 3
Control: ActGal4, Gal80ts, /Cyo-GFP
Plk4KD: ActGal4, Gal80ts, /Cyo-GFP; Plk4mut /TM6 Tb X +/Cyo-GFP; GFP- Plk4KD, Plk4 mut/ TM6 Tb
Plk4WT: ActGal4, Gal80ts, /Cyo-GFP; Plk4mut /TM6 Tb X +/Cyo-GFP; GFP- Plk4WT, Plk4 mut/ TM6 Tb
Crosses were maintained at 18 °C for 4 days after egg laying and transferred to 29°C for 48hrs.
SFigure 4
Control: RFP-Fzr/Cyo-GFP; Plk4mut/TM6Tb X Ase-Gal4, Tub-GFP/Cyo-GFP; Plk4mut/TM6Tb
Plk4KD: RFP-Fzr/Cyo-GFP; GFP- Plk4KD, Plk4 mut X Ase-Gal4, Tub-GFP/Cyo-GFP; Plk4mut/TM6Tb
Plk4WT: RFP-Fzr/Cyo-GFP; GFP- Plk4WT, Plk4 mut X Ase-Gal4, Tub-GFP/Cyo-GFP; Plk4mut/TM6Tb
Wf
Crosses were maintained at 25°C
SFigure 5
Control: ActGal4, Gal80ts, /Cyo-GFP
Plk4KD: ActGal4, Gal80ts, /Cyo-GFP; Plk4mut /TM6 Tb X +/Cyo-GFP; GFP- Plk4KD, Plk4 mut/ TM6 Tb
Crosses were maintained at 18 °C for 4 days after egg laying and transferred to 29°C for 48 hrs.
GFP-Tub, AseGal4/Cyo-GFP; X Ubq RFP-Sas6
Crosses were maintained at 25°C

Live Imaging

WorGAL4 or AseGAL4 drivers were used to induce the transgene expression only in NBs. In general, the over-expression of any GFP-Plk4 or RFP-Spd2 proteins leads to the formation of large green/red aggregates that are frequently segregated into the GMCs. Other smaller aggregates or green particles can often been seen in NBs and GMCs. In all the movies analyzed and presented in this article, the centrosome or centriole were distinguished by its capacity to nucleate MTs, or through its position at spindle poles or association with the spindle during mitosis in the the period of the time-lapse (even if not included in the stills). In certain cases, the timeframe where it is possible to distinguish a centriole or centrosome is not included in the Figures shown, but we carefully characterize centrosome/centriole behavior and dynamics to identify the same centrosome/centriole in different time frames. Mid third instar larval brains were dissected in Schneider's *Drosophila* medium (21720-024, Gibco, ThermoScientific) supplemented with 10% heat-inactivated fetal bovine serum (10500, Gibco, ThermoScientific), penicillin (100 units ml^{-1}) and streptomycin (100 $\mu g\ ml^{-1}$) (penicillin–streptomycin 15140, Gibco, ThermoScientific) (hereafter referred to as live imaging medium). Brains were placed on a glass-bottom 35 mm dish (P35G-1.5-14-C, Mat Tek Corporation, MA, USA) with 10 μl of medium, covered with a permeable membrane (Standard membrane kit, YSI, OH, USA) and sealed around the membrane borders with Voltalef oil 10S (VWR BDH Prolabo). One or two brain lobes were recorded using a Yokagawa CSU-X1 spinning head mounted on a Nikon TiE inverted microscope. The microscope was equipped with an EMCCD Evolve 512 × 512 (Photometrics, AZ, USA) and controlled by the Metamorph software 7.7 (Molecular devices). Four-dimensional z-stacks of 18–26μm at 0.75-μm intervals were acquired every 30 or 60 s using an x60, NA 1.4 oil-immersion objective. The same laser power and acquisition settings were kept for all time lapse acquisitions. Images were processed with Fiji (NIH) and Adobe Photoshop.

Immunohistochemistry and Antibodies

Third instar larval brains were dissected in PBS and fixed in 4% formaldehyde in PBS for 30 min. After fixation, brains were transferred to 45% acetic acid (diluted in water) for 15 sec and then to 60% acetic acid (diluted in water) for 3 min. Brains were then mounted onto a slide, squashed and immediately flash-frozen in liquid nitrogen, followed by a further fixation with ice-cold methanol, at -20C for 7 min. Next, brains were rehydrated in PBS + 0.1% Triton X-100 (T9284, Sigma), 3 times for 15 min. Once dried, brains were

incubated overnight at 4℃ with the primary antibody solution diluted in PBS + 0.1% Triton, in a humid chamber. Brains were then rehydrated in PBS + 0.1% Triton, 3 times for 15 min, allowed to dry and incubated for 2h at 25℃ with the secondary antibody solution in PBS + 0.1% Triton, in the dark, in a humid chamber. Next, brains were rehydrated in PBS + 0.1% Triton, 3 times for 15 min and incubated 15 min with Hoechst 33342 (Invitrogen), at 0.5μg/ml in PBS + 0.1% Triton. Finally, once dried, brains were mounted in mounting medium (1.25% N-propyl gallate, 75% glycerol, 25% H_20).

For 3D SIM imaging or confocal imaging, whole mount third instar larval brains were dissected in PBS and fixed in 4% paraformaldehyde diluted in PBS + 0.1% Triton for 30 min. Brains were then permeabilized with 3 washes in PBS + 0.3% Triton. Next, a blocking step followed, by incubation in PBS + 10% NGS for 30 min. Next, brains were incubated with primary antibody solution (PBS + 0.3% Triton), first a few hours at room temperature on gentle agitation, and then overnight at 4℃. Brains were then washed 3 times in PBS + 0.3% Triton, followed by incubation with secondary antibody solution, overnight at 4℃ which also included a phalloidin conjugated probe to label the cell membrane. After 2 washes in PBS + 0.3% Triton (5 min each), brains were incubated with Hoechst 33342 (0.5ug/ml in PBS+0.3% Triton) for 30 min before a final wash in PBS. Finally, brains were rapidly washed 3 times in PBS. They were mounted in mounting medium as described above. For the 3D SIM analysis, the appropriate NBs in interphase were chosen based on the presence of a large intact nucleus. The apical cortex was identified by the presence of a centrosome/centriole in Ctrl and $Plk4^{KD}$ brains and by its position relative to GMCs. In $Plk4^{WT}$ NBs, centrioles are positioned towards the basal hemisphere.

Primary antibodies used: rabbit anti-Spd2 (1:500; (Dix and Raff, 2007), guinea pig anti-Cnn (1:1000, (Lucas and Raff, 2007), rabbit anti-PPHC (Plp) (Martinez-Campos et al., 2004), mouse anti-α-Tubulin (DM1α) (1:500, Sigma Aldrich), rabbit anti-aPKC (1:100, SC116, Santa Cruz) and mouse anti-Prospero (1:20, DSHB). Secondary antibodies used: Alexa Fluor 488, Alexa Fluor 546 and Alexa Fluor 647 (Molecular Probes, ThermoScientific), Phalloidin conjugated probes (R415) for F-actin labelling in red, from molecular probes (Thermo Fisher) were used to label the cell membrane, RFP and GFP Boosters (Atto 594 and Atto 488) (1:100, Chromotek).

Drug Treatments

For analysis of centrosome position in NBs, third instar brains were placed in PBS or PBS supplemented with colcemid -demecolcine (D7385, Sigma Aldrich) (50μM final concentration) for exactly 1h at 25℃. Brains were then fixed as described above for whole mount preparations.

To inhibit the proteasome, Bortezomib (PS-341, Selleck Chemicals) was added to the live imaging medium at a concentration of 50μM, a concentration that led to mitotic arrest in NBs. Brains were fixed after 2 hours of incubation in the medium supplied with the drug. Control brains were incubated in live imaging medium with 1% DMSO. Brains were then fixed as described above for whole mount preparations.

For live imaging, third instar larval brains were dissected in live imaging medium and then incubated in live imaging medium implemented with the appropriate drug. To depolymerize MTs, demecolcine (D7385, Sigma Aldrich) was added to the medium at a concentration of 50 μM as described previously (Januschke and Gonzalez, 2010). We noticed that fluorescence intensity of centriolar tagged proteins used in this study- RFP-Sas6 and GFP-$Plk4^{KD}$ decreases at the centriole, indicating a possible instability of these proteins in the absence of centriolarMTs. For actin depolymerization, cytochalasin D (C8273, Sigma Aldrich) was added to the medium at a concentration of 50 μM. After dissection, brains were placed on the glass-bottom dish in 10 μl of live imaging medium with demecolcine or cytochalasin D. Brains were filmed immediately after.

Western Blot of Spd2 Transgenic Lines

Twenty third instar larval brains of each genotype were dissected in cold PBS supplied with 1% protease inhibitor cocktail (P8340, Sigma) and 1mM PMSF (P7626, Sigma) and collected in a tube. 20 ml of sample buffer was added to the brains and the tissues were stripped with the help of blunt forceps on ice to induce mechanical dissociation. Samples were boiled at 70°C for 10min. Samples were run in 10% Bis/Tris gel in MOPSSDS buffer at 180V (Np0301 and NP0001 from NuPAGE-ThermoFIsher) and transferred fir 1h at 100V in the cold using 0.2 μm NC nitrocellulose (GE Healthcare Life Science). Membranes were then blocked in PBS supplemented with 0.1% Tween20 (PBST) and 10% dried milk powder for 30 min followed by incubation O/N 4℃ with Spd2 primary antibody at 1:500 (Dix and Raff, 2007) , diluted in PBST with 3% dried milk powder. Membranes were washed 4 times for 10min in PBST and then incubated for 2h at room-temperature with a Rabbit secondary antibody conjugated to Horseradish peroxidase (HRP) (# G21234, Life Technologies) diluted in PBST with 3% dried milk powder. The secondary antibody solution was then removed and membranes washed 5 times for 10min in PBST. Finally, membranes were incubated with SuperSignalTM West Pico Chemiluminescent Substrate (34080, Termo ScientificTM) and revealed using the BioRad Chemidoc MP system. Images were analyzed using ImageLab software.

In Vitro Kinase Assays and Mass Spectrometry

Bacterially-expressed constructs of *Drosophila* Plk4 (amino acids 1–317) C-terminally tagged with FLAG-His_6 and *Drosophila* Spd2 N-terminally tagged with either Glutathione S-Transferase (GST) or Maltose-binding protein (MBP) were purified on HisPur resin (ThermoFisher), glutathione resin (NEB) and amylose resin (NEB), respectively, according to manufacturer's instructions. Prior to assay, purified proteins were resolved by SDS-PAGE and scans of the Coomassie-stained gels analyzed by densitometry (ImageJ, NIH) to determine protein purity. Total protein concentrations of the same reagents were measured by Bradford assay (BioRad). The total protein and purity measurements were used to calculate the concentration of each protein reagent. (Contaminants and proteolytic fragments are excluded by this calculation.). In vitro phosphorylation assays were performed by incubation with

100 μM ATP for 60-90 min at 24°C in reaction buffer [40 mM Na HEPES (pH 7.3), 150 mM NaCl, 5 mM $MgCl_2$, 0.5 mM $MnCl_2$, 1 mM DTT, 10% (by volume) glycerol]. Samples were resolved by SDS-PAGE, and proteins visualized by Coomassie staining. Phosphorylation of protein substrates was evaluated by including γ-^{32}P-ATP in assays and, subsequently, the presence of radiolabeled substrates detected by autoradiography of dried gels. Phosphorylated residues within proteins were identified by tandem mass spectrometry (Table S1) of purified bacterially-expressed proteins phosphorylated *in vitro* (described above in 'Generation of Spd2 fragments') in the presence of non-radioactive ATP and performed at the Arizona Proteomics Consortium (University of Arizona). Samples of Spd2 were reduced (10μM dithiothreitol, 55°C, 1hr), alkylated (55mM iodoacetamide, 24°C, 45min), and trypsin digested (~1μg trypsin, 37°C, 12hrs) in-gel, and then extracted. Peptide samples were desalted using ZipTip 0.6μL C_{18} resins (EMD Millipore, Billerica, MA). The peptides were then separated by HPLC on a C_{18} analytical column, ionized by electrospray ionization (ESI) in positive mode, and analyzed on a LTQ Orbitrap Velos (Thermo Electron Corp., San Jose, CA) mass spectrometer. All LC MS analyses were carried out in ''data-dependent'' mode in which the top 6 most intense precursor ions detected in the MS1 precursor scan (m/z 300-2000) were selected for fragmentation via collision induced dissociation (CID). Precursor ions were measured in the Orbitrap at a resolution of 60,000 (m/z 400) and all fragment ions were measured in the ion trap.

RNAi of *Drosophila* S2 Cells

Cells were plated at 50% confluency and treated with 10 μg/day dsRNA for 7 days. Cells were passaged before they reached ~90% confluency. On day 5, cells were transfected with 2 μg of plasmid and 10 μg dsRNA using the Nucleofector II (Lonza). Transgenes were expressed by treating with 0.5 mM CuSO4 for 24 hours.

Co-Immunoprecipitation and Immunoblotting

GFP-binding protein fused to Human IgG was coupled to Protein-A conjugated Dynabeads (Invitrogen) and cross-linked to the beads with dimethyl pimelimidate dihydrochloride (Sigma). Beads were blocked overnight in PBS-0.1% Triton X-100 + 1% BSA. S2 cells were lysed in IP buffer (50 mM Tris pH 7.2, 125 mM NaCl, 1 mM EGTA, 0.5% Triton X-100, and 0.4 mM NaN_3, 1 mM dithiothreitol (DTT), 1mM phenylmethylsulfonyl fluoride (PMSF), 1 μg/mL soybean trypsin inhibitor (SBTI), and SIGMAFAST protease inhibitor cocktail (Sigma), then precleared by centrifugation at 10,000 rcf for 5 minutes at 4°C. A sample of cleared lysate was used for input blots. Beads were equilibrated in IP buffer, then 50 μL of beads were added to the remaining lysate and rocked at 4C for 30 minutes. Beads were washed 4x with IP buffer by resuspension and then harvested with a magnet between washes. Beads were transferred to a new tube during the final wash. Samples were eluted by boiling in Laemmli buffer (40 μL of 2x). Inputs and IPs were resolved by SDS-PAGE and transferred to nitrocellulose membrane, then analyzed by Western blot using mouse anti-GFP (1:3000, clone JL-8; Clontech Laboratories, Catalogue #632381), mouse anti-α-Tubulin (1:3000, clone DM1a; Sigma, Catalogue #T9026), guinea pig anti-Spd2 (1:500, polyclonal), mouse anti-HA (1:1500, Clone HA-7; Sigma, Catalogue #H3663), or mouse anti-V5 (1:1500; Invitrogen; Catalogue #46-0705) primary antibodies, followed by fluorescently-labeled goat anti-mouse (1:3000; Li-COR IRDye 800CW, Catalogue #926-32210) or donkey anti-guinea pig (1:3000; Li-COR IRDye 800 CW, Catalogue #926-32411) secondaries. Detection was performed on a LiCOR odyssey cL-X fluorescent imaging system at medium quality and 84 nm resolution.

Synthesis of Spd2 dsRNA

dsRNA was synthesized by *in vitro* T7 transcription using PCR product amplified from Spd2 EST (CG17286, Clone ID LD24702, DGC EST Library 1.0) with the primers Spd2-UTR-For: 5′ – TAATACGACTCACTATAGGGGTTTTCGCGTTCGCACTGCAAACTGTAA CTGTTTAAGGACAAAGCGGATTTGTTTTATTTGTGCCTGC and Spd2-UTR-Rev: 5′ – TAATACGACTCACTATAGGGCTTTTAGGAAA CAAGCG.

Image Acquisition

Images of squashed preparations were collected with a x100 objective on a Leica DM6B epifluorescence microscope, this microscope was equipped with an ORCA-Flash4.0 V2 Digital CMOS camera (Hamamatsu) and controlled by the Metamorph software 7.7 (Molecular devices). Images of whole mount brain lobes were acquired on a Nikon A1R inverted TiE confocal microscope with a 40X 1.3NA or a X60 1.4 NA objective in NIS Element software. For the characterization of Spd2 and Fzr localization in interphase centrioles, images were acquired with a N-SIM Nikon microscope in 3D SIM mode before image reconstruction using the NIS Elements software (Gustafsson et al., 2008). The system is equipped with an APO TIRF SR 100x 1.49NA oil immersion, a laser illumination (488nm 200mW, 561nm 100mW, 640nm 100mW) and an EMCCD DU-897 Andor camera. Images were acquired with the following protocol, a Z stack (0.12 micron steps) was acquired. Images were then reconstructed using Nikon elements software.

QUANTIFICATION AND STATISTICAL ANALYSIS

Characterization of Centriole Behavior

The characterization of centriole movement was performed on raw data taking into account the Z-stacks required to follow centriole behavior in x, y and z. Z-stacks were used to generate projections to follow the centriole behavior over time. In Ctrl cells, after mitosis, the two centrioles display stereotypic movements as described previously (Rebollo et al., 2007; Rusan and Peifer, 2007) and this behavior was taken for the basis of characterization of centriole behavior in the different genotypes. Centrioles were considered ''Apical'' when behaving as Ctrl apical centrioles- maintaining a stable and fixed position closer to the apical cell cortex throughout

interphase. The apical cell cortex was established by the position of the large aster, at the end of telophase, typical of the asymmetric spindle in NBs. Centrioles were categorized as apical mobile when they were maintained within the apical hemisphere (top half of the cell), Centrioles that moved away from the apical cortex and were positioned towards the basal hemisphere (bottom half of the cell) were considered as ''Basal-like'' centrioles. Frequently, they displayed a random jumping movement). In certain cases, the NB moved and the neighboring cells were used as landmarks to position the apical cortex at different time points. . For the characterization of centriole behavior in the different Plk4 transgenes, 20 NBs from 3 Ctrl brains, 26 NBs from 7 $Plk4^{KD}$ brains and 20 NBs from 7 $Plk4^{WT}$ brains were analyzed. In the same type of analysis in the Fzr^{mut} background, 12 NBs from 3 Fzr^{mut} brains and 18 NBs from 5 Plk4KD,Fzr^{mut} brains were analyzed.

Stabilization and Tracking Centriole Dynamics in Time-lapse Movies

To stabilize the full set of images that comprise each time-lapse movie, we used the ''SetLandmark'' and ''StabilizeMovie'' plugins from ImageJ. With the ''SetLandmark'' we defined a landmark on each frame to identify the apical and basal axis of each NB cell. Subsequently, translations and rotations were applied to align the center of the previously established landmarks at the center of the image. Centrosome/centriole tracking was performed with the ''Tracking'' plugins from ImageJ. In each time frame the centriole was identified and labelled manually in order to allow tracking of their movement. After this step, we used ''PrintTracking'' from imageJ to draw the tracking of each centrosome/centriole.

Analysis of Spindle Orientation after Two Consecutive Mitosis

Analysis of spindle orientation was performed on time-lapse movies where two consecutive mitosis of the same NB could be identified. In both mitosis spindle axis was determined at early anaphase. The angle between the two spindles was measured using the ''Angle tool'' from Fiji (NIH).

Analysis of Spindle Orientation in Mitotic NBs

Analysis of spindle orientation was performed on metaphase or anaphase NBs that contained a clear aPKC crescent. The angle between the spindle and the middle of the aPKC crescent was determined using the ''Angle tool'' from Fiji (NIH).

Analysis of Centrosome Position in NBs

We only analyzed NBs were a clear group of GMCs could be seen to identify the position of the apical cortex at the opposite side of the GMCs. First, a line was drawn from the apical cortex to the basal to measure the apical-basal axis length with the Fiji (NIH) ''Straight line'' tool. Then a second line, positioned at the same position than the first line (at the apical side), was drawn till it reached the centrosome, labelled with two centrosome markers (only one is shown in the Figure). The two values for each NB (apical-basal axis length and centrosome distance from the apical cortex) were plotted on an excel sheet. Centrosome position was then calculated by dividing the second measure by the first one.

Characterization of Centrosomal Protein Levels in Interphase Centrioles

Quantification of the levels of centrosome proteins in interphase were performed in at least ten NBs for each genotype from 3 independent experiments. For each set of immunostaining experiments, the same acquisition settings were kept for all conditions. Images were analyzed with Fiji (NIH) and quantifications done as follows. The fluorescence mean grey value (F_c) was measured by drawing the area occupied by the protein of interest with the freehand tool in a single Z plane, representing the center of the centrosome. The cytoplasmic fluorescence (F_{cy}) was measured by drawing a round area as big as about one-fourth of the cell size and then subtracted from Fc to obtain the net fluorescence of the centrosome (V_c=F_c-F_{cy}). The signal of the background (F_{bkg}) outside the cell was also measured to obtain the net fluorescence of the cytoplasm (V_{cy}=F_{cy}-F_{bkg}). Finally, centrosome enrichment was measured as ratio between V_c and V_{cy} (V_c/V_{cy}).

Statistical Analysis

Statistical analysis was performed with GraphPad Prism 7. A two-tailed unpaired t-test was used to assess statistical differences. All details of statistical analyses, including n and p values, are found in the text and Figures. All results are presented as mean ± SD.

Developmental Cell, Volume *50*

Supplemental Information

Plk4 Regulates Centriole Asymmetry and Spindle Orientation in Neural Stem Cells

Davide Gambarotto, Carole Pennetier, John M. Ryniawec, Daniel W. Buster, Delphine Gogendeau, Alix Goupil, Maddalena Nano, Anthony Simon, Damien Blanc, Victor Racine, Yuu Kimata, Gregory C. Rogers, and Renata Basto

Figure S1- Gambarotto et al

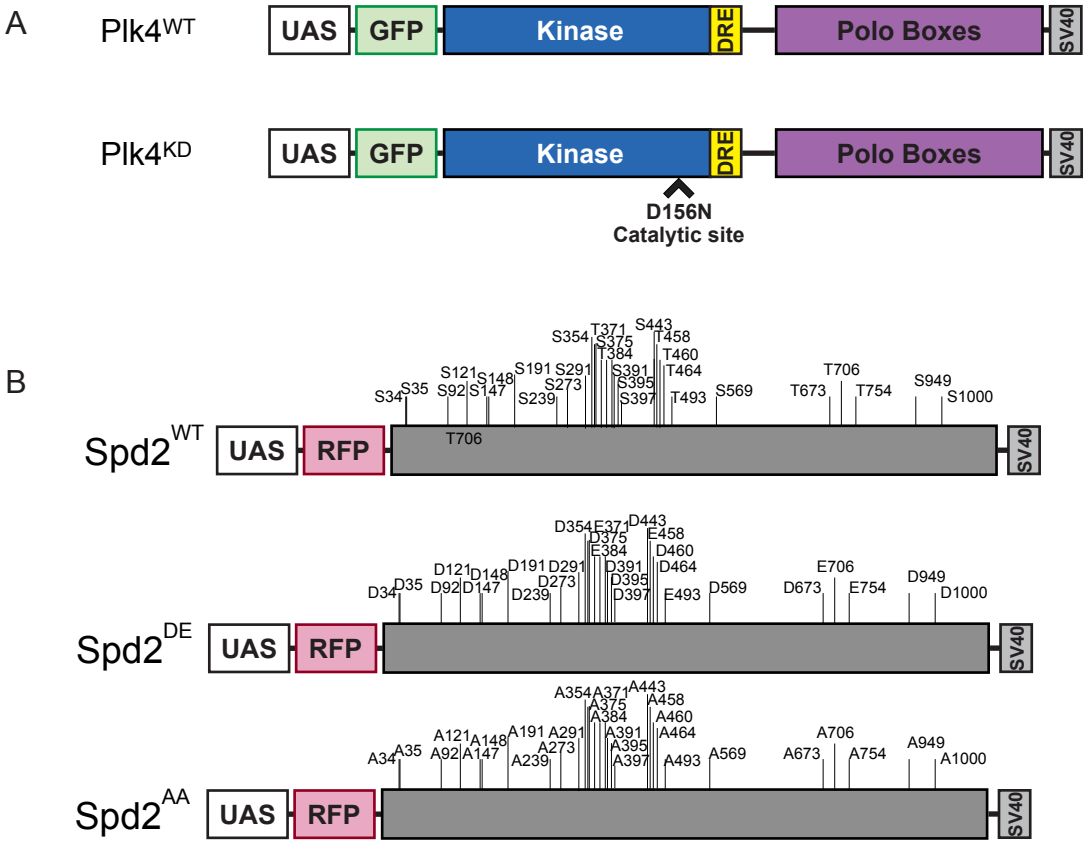

Figure S2- Gambarotto et al

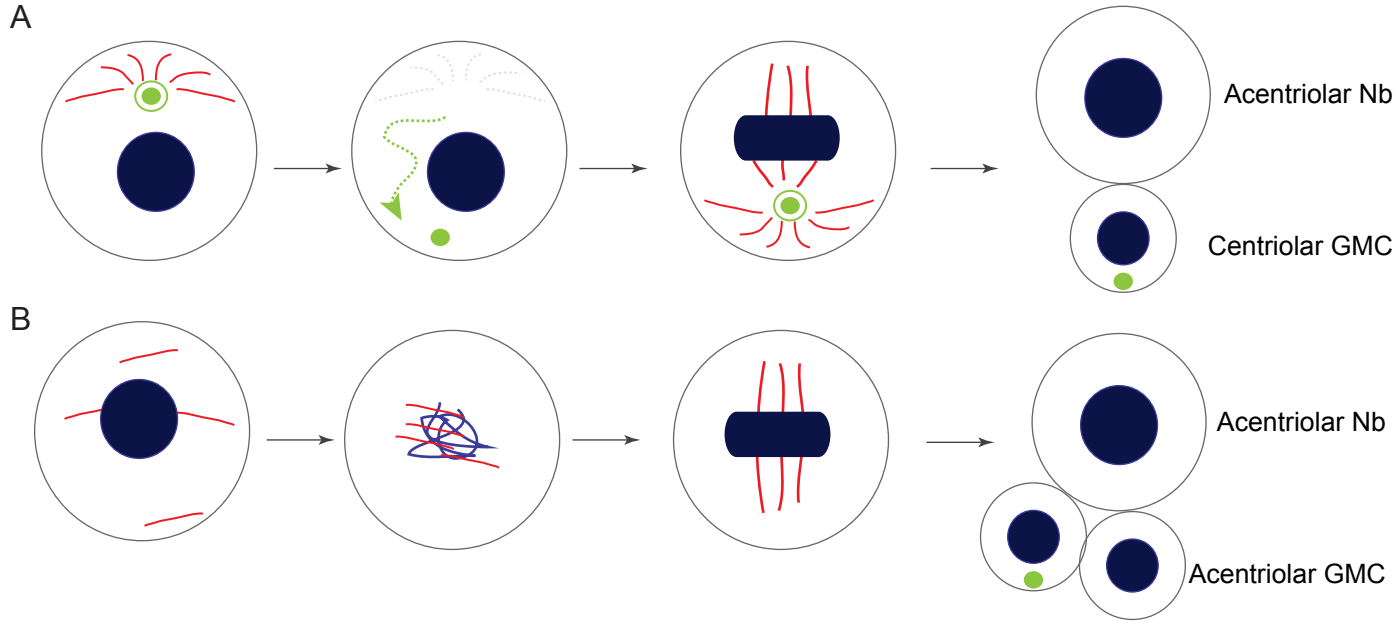

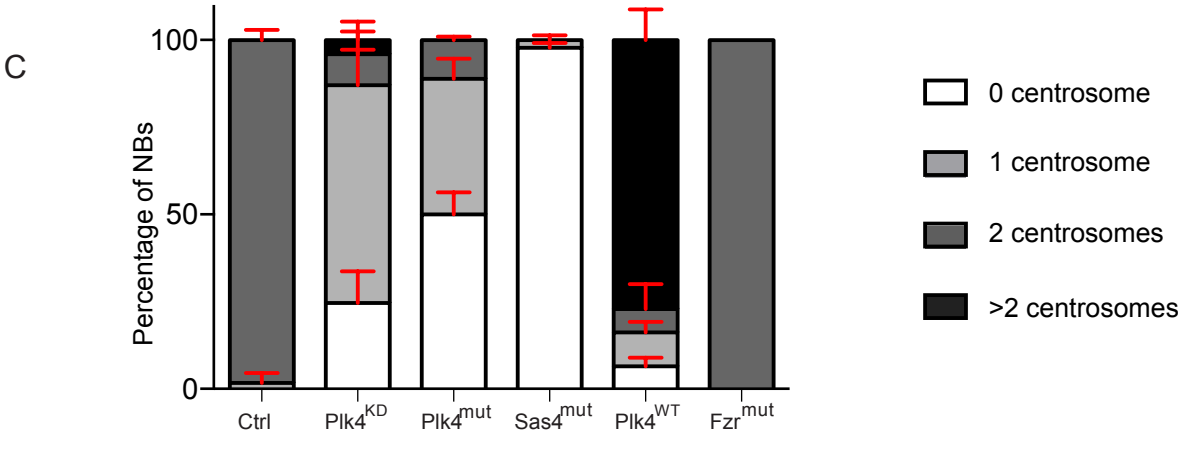

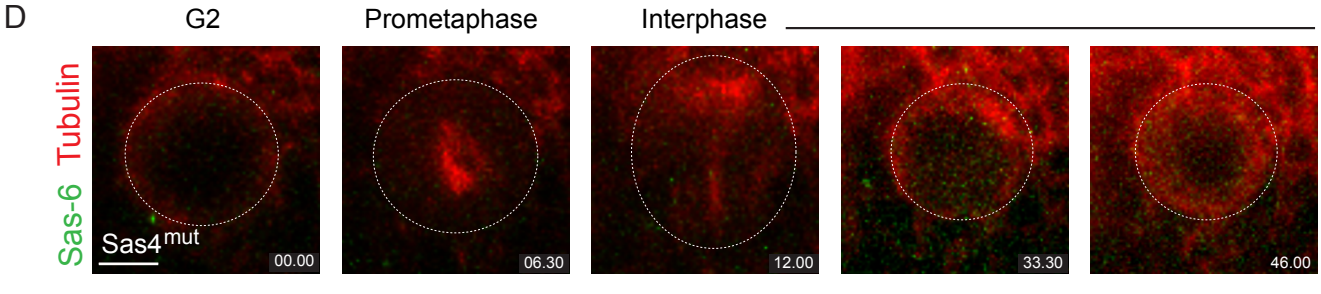

Figure S3- Gambarotto et al

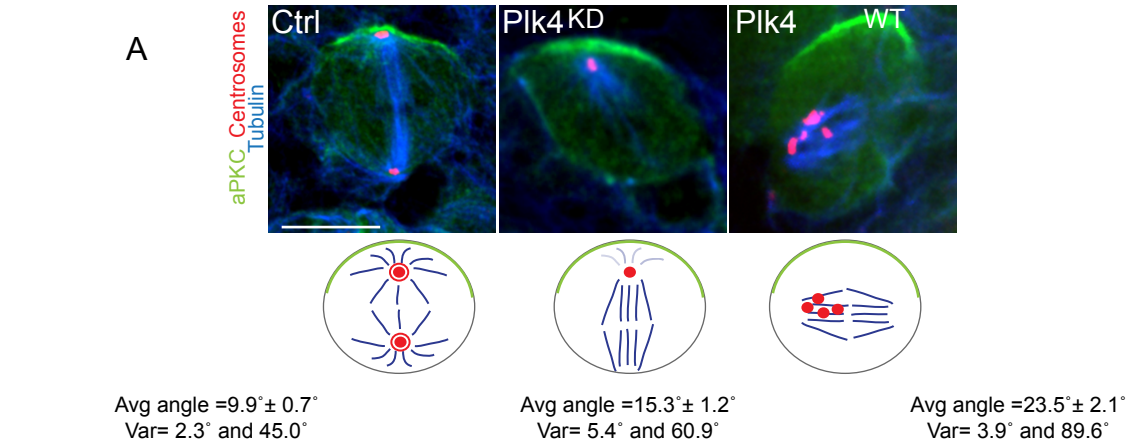

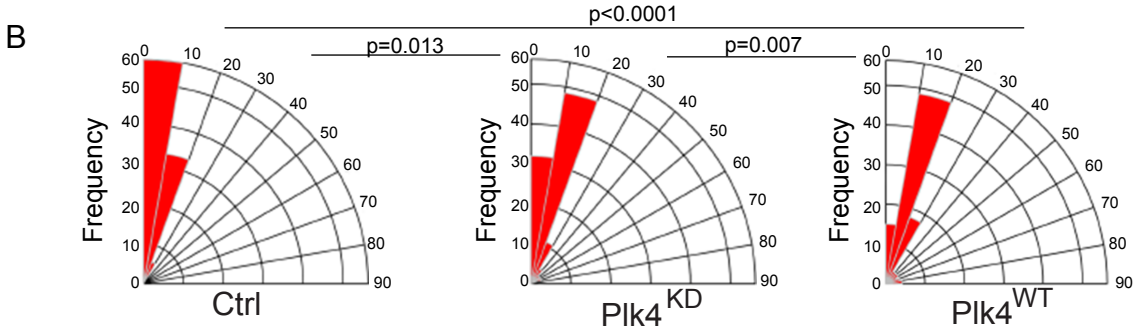

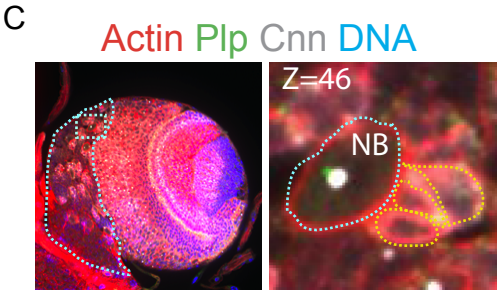

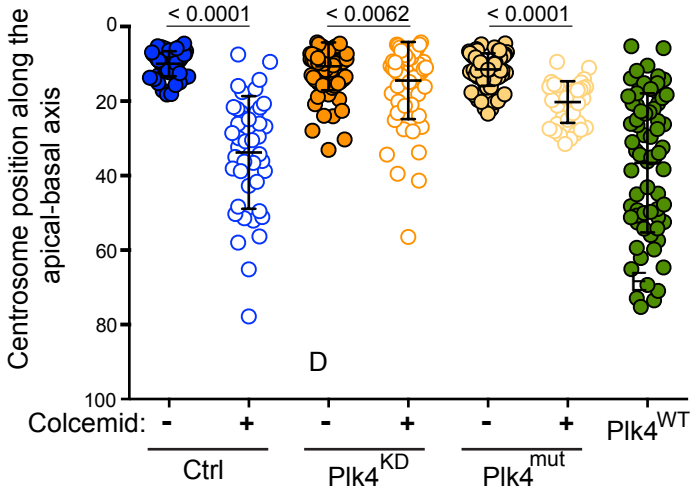

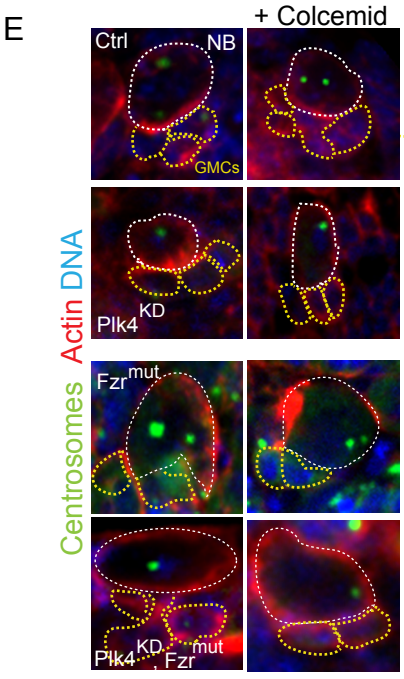

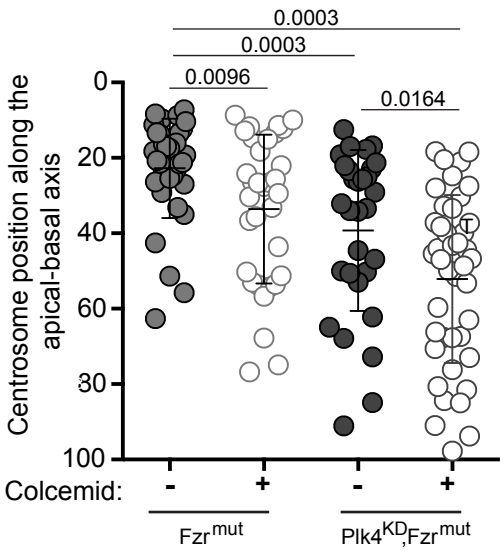

SFigure S4 - Gambarotto et al

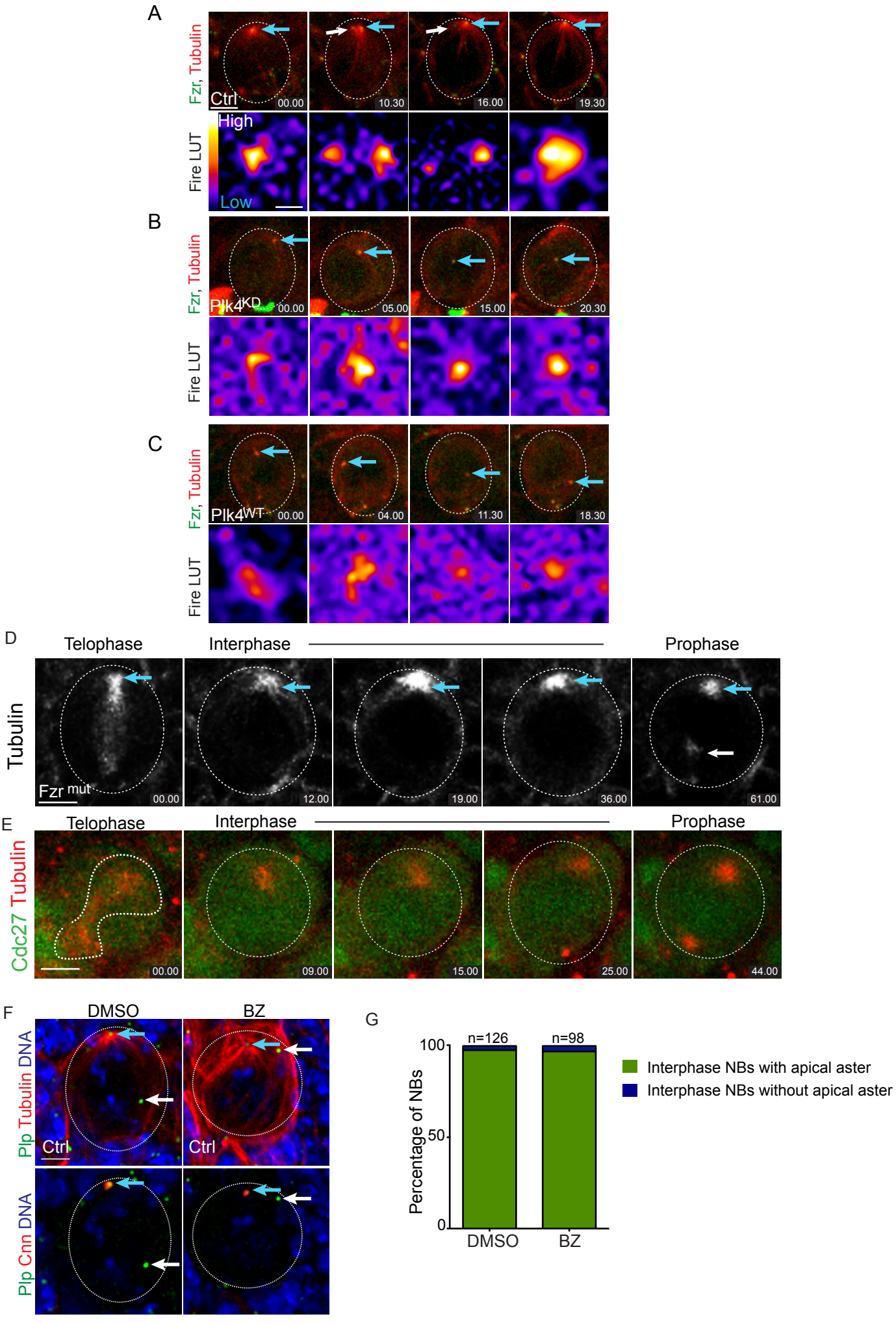

Figure S5 - Gambarotto et al

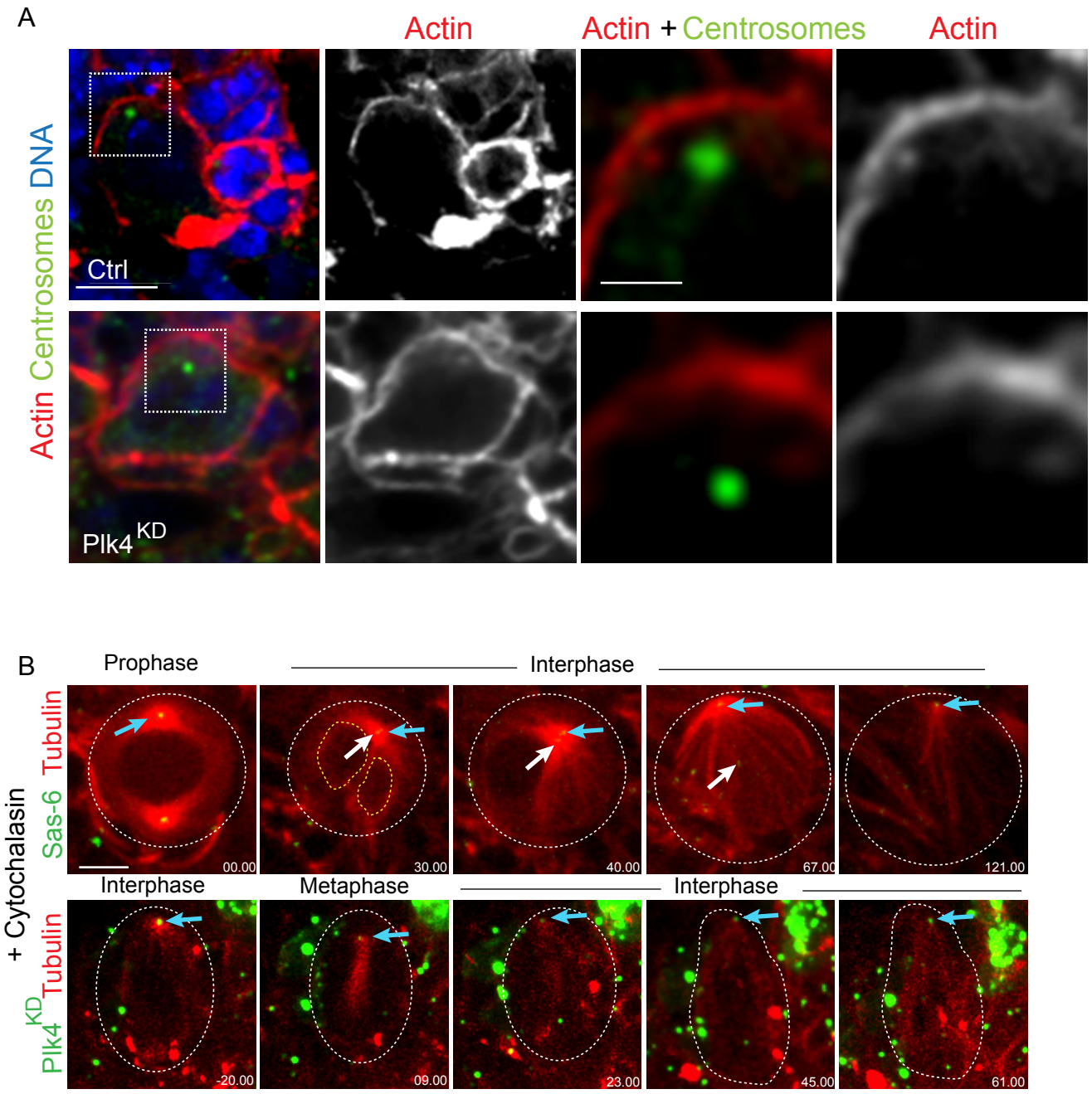

Figure S6- Gambarotto et al

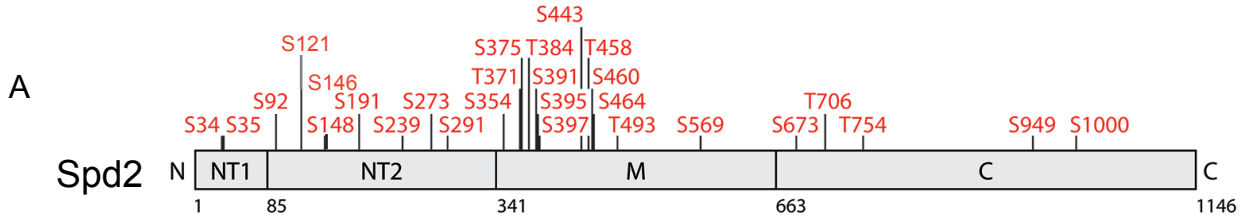

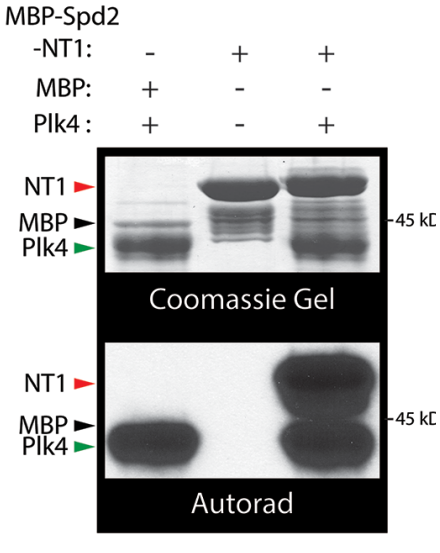

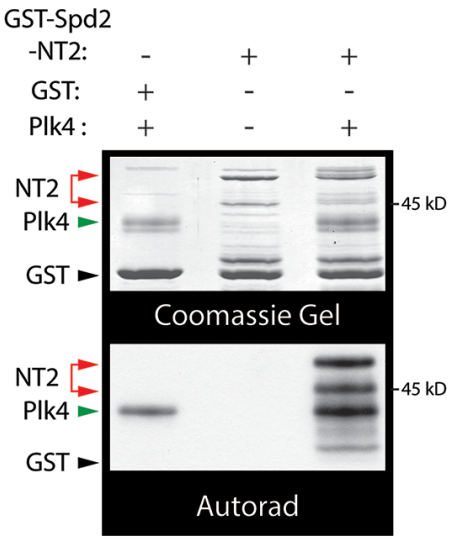

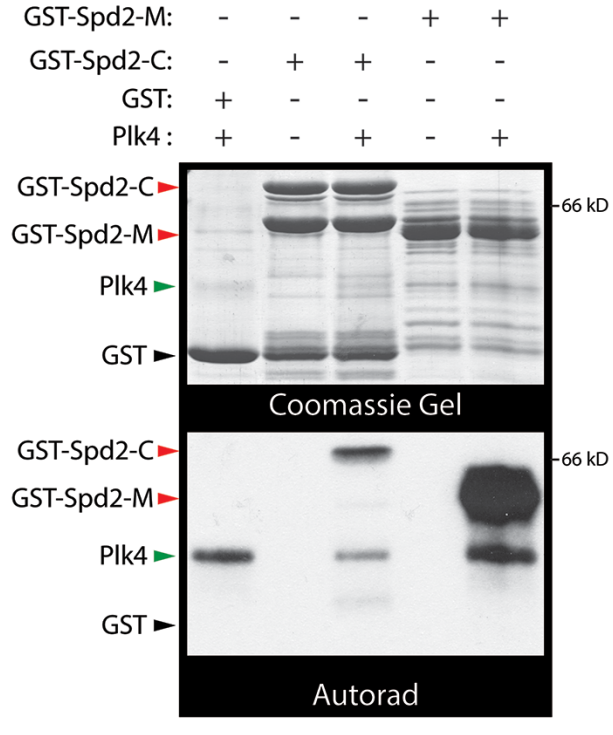

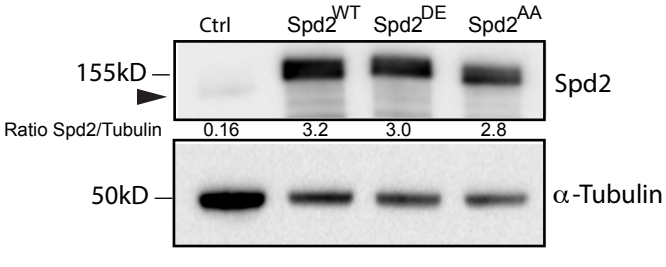

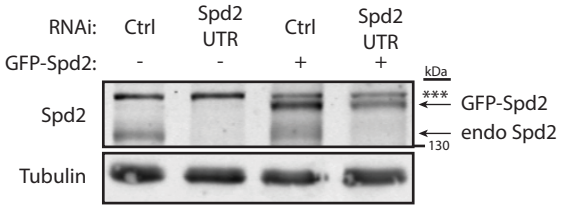

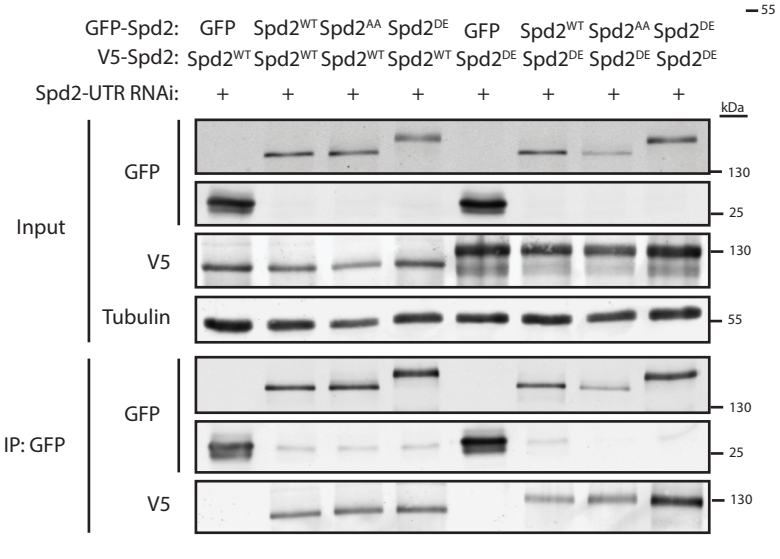

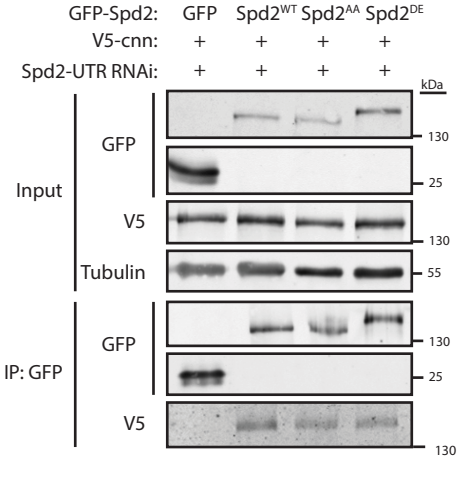

SUPPLEMENTARY FIGURE and MOVIE LEGENDS

Supplementary Figure 1 – Diagram of Plk4 constructs analyzed

(A, B) Transgenes were under the control of the UAS promoter and their expression induced through the UAS/GAL4 system. (A) The UAS sequence was fused to the GFP coding region, upstream of Plk4 WT cDNA containing the entire coding region from the initial starting ATG to the stop codon, while the $Plk4^{KD}$ contains a mutation in the kinase catalytic site of Aspartic Acid 156 to Asparagine (D156N) that prevents centriole duplication, (Brownlee et al., 2011, Habedanck et al., 2005, Holland et al., 2010). The GFP and Plk4 sequences are spaced by a linker of 12 bp encoding G-G-T-G-G-T). (B) The UAS sequence was fused to the RFP coding region upstream of $Spd2^{WT}$ or $Spd2^{DE}$ or $Spd2^{AA}$ coding regions. The RFP and Spd2 sequences are spaced by a linker of 12 bp encoding G-G-T-G-G-T). Related with Figure 1 and Figure 4

Supplementary Figure 2 – Analysis of centrosome numbers in NBs of centriole mutants

Related with Figures 1-3

(A, B) Schematic explaining the absence of centrioles in NBs of Sas-4 mutants ($Sas\text{-}4^{mut}$). (A) At mitotic exit, the NB inherits a single unduplicated centriole. Through centriole maturation, the single centriole becomes a mother centriole and, consequently, loses apical anchoring and starts moving randomly into the basal side throughout interphase. In the following mitosis, it will most likely form the pole that will be segregated into the GMC giving rise to an acentriolar NB. (B) In the following mitosis, the acentriolar NB will form an acentrosomal spindle, mainly using the chromatin-mediated microtubule assembly pathway. (C) Graph of centriole numbers in NBs of the indicated genotypes. Error bars represent standard error of the mean.(D) Still images from time-lapse movies of a $Sas\text{-}4^{mut}$ NB. Tubulin is shown in red and RFP-Sas-6 in green. The $Sas\text{-}4^{mut}$ NB lost its centrioles in the previous cell cycles as judged by the absence of RFP- Sas-6 positive dots. Time is shown in minutes. Scale, 3 μm.

Supplementary Figure 3 – Analysis of spindle positioning in mitotic NBs

Related with Figures 2-3

(A) Immunostaining of Ctrl, $Plk4^{KD}$ and $Plk4^{WT}$ NBs using antibodies against aPKC (green), tubulin (blue) to label the mitotic spindle and centrosomes (red). The diagrams

below recapitulate spindle position relative to the aPKC crescent. Scale, 4 μm. (B) Quantification of mitotic spindle orientation during mitosis in Ctrl, $Plk4^{KD}$ and $Plk4^{WT}$ NBs. (C) On the left, picture of whole mount brain lobe projection to illustrate NB and GMC organization within the central brain revealed by actin labeling with phalloidin (shown in red) and labeled with antibodies against Plp and Cnn (green and white respectively) to label centrosomes. DNA in blue. The dashed blue lines surrounds the central brain region and the dashed square illustrates the NB-GMC progeny in the higher magnification on the right. (D) Dot plot of centrosome positioning along the apical basal axis with (+) and without (-) colcemid for the indicated genotypes (Ctrl- 9.9±0.4 Ctrl+ 33.8±2.2; $Plk4^{KD}$-10.6±0.7 $Plk4^{KD}$+ 14.5±1.3; $Plk4^{mut}$- 11.5±0.5 $Plk4^{mut}$+ 20.3±0.9; $Plk4^{WT}$ 36.6±18.7). Error bars represent means ± SD from at least 3 independent experiments. Statistical significance was assessed by unpaired t-test. (E) Immunostaining of Ctrl ,$Plk4^{KD}$, Fzr^{mut} and $Fzr^{mut}Plk4^{KD}$ NBs, treated with (right) or without (left) colcemid. Plp is shown in green, phalloidin-labed actin in red and DNA (blue). Scale, 5μm. (F) Fzr^{mut}- 22.7±2.2 Fzr^{mut} + 33.6±3.4; $Plk4^{KD}$, Fzr^{mut} - 39.2±3.9 $Plk4^{KD}$, Fzr^{mut} +52.1±3.4. Error bars represent means ± SD from at least 3 independent experiments. Statistical significance was assessed by unpaired t-test.

Supplementary Figure 4 – Analysis of the role of Fzr in centriole apical anchoring

Related with Figures 2-3

(A-C) Images from time-lapse movies of Ctrl, $Plk4^{KD}$, and $Plk4^{WT}$ NBs expressing RFP-Fzr. For each genotype, the top panel shows Tubulin (red) and RFP-Fzr (green). The bottom panels show a higher magnification fire LUT representation of RFP-Fzr levels at the centriole (purple=low levels, white=high levels). The blue arrow points to the apical centrosome or centriole inherited by NB at the end of mitosis, while the white arrow points to the basal centriole. Time, minutes. Scale, 4μm. (D) Images from time-lapse movies of Fzr^{mut} NBs. Tubulin (grey). Blue arrows point to the apical centriole, which maintains a strong aster throughout interphase. Time, minutes. Scale, 4 μm. (E) Images from time-lapse movies of GFP-Cdc27 NBs. Tubulin (red) and GFP-Cdc27 (green). During interphase, GFP-Cdc27 does not localize to centrosomes. Time, minutes. Scale, 3 μm. (F) Confocal images show the maintenance of an apical aster in Ctrl NBs incubated either with DMSO (left) or the proteasome inhibitor BZ (middle). Brains were immunostained for Plp (green), tubulin (red in top panels) and Cnn (red in bottom panels). DNA(blue). Scale, 4 μm. (G) Graph shows the percentage of interphase Ctrl NBs

that display an apical centriole and aster after incubation with DMSO (n=126 NBs) or BZ (n=98 NBs).

Supplementary Figure 5 - Centrosomes in *Drosophila* NBs are not associated with an actin-based structure

Related with Figure 3

(A) Immunostaining of Ctrl (top) and Plk4^{KD} (bottom) NBs stained with Phalloidin to label the actin cortex (red) and immunostained for centrosomes (green). DNA, blue. The insets on the right show higher magnification regions of the centrosome-cortex region Scales, 4 mm and 1mm. (B) Images from time-lapse movies of Ctrl (expressing Sas-6 GFP) and Plk4KD NBs expressing tubulin-RFP in the presence of cytochalasin D. The blue arrow points to the apical centrosome (in Ctrl) or centriole (in Plk4KD). The white arrow points to the basal centriole in the Ctrl NB. Time, minutes. Scale, 4 μm.

Supplementary Figure 6 – Plk4 extensively phosphorylates Spd2, and Spd2 phospho-mutations do not effect Spd2 homodimerization or its association with with Cnn

Related with Figure 4-5

(A) Spd2 was bacterially-expressed and purified as four fragments that collectively span the entire protein: MBP-Spd2-NT1 (amino acids 1-84), GST-Spd2-NT2 (amino acids 85-340), GST-Spd2-M (amino acids 341-662), and GST-Spd2-C (amino acids 663-1146). Spd2 fragments were incubated with Plk4 kinase domain (amino acids 1-317) and MgATP, then resolved by SDS-PAGE, and the excised Spd2 bands processed for analysis by tandem mass spectrometry (MS/MS) to identify phosphorylated serine and threonine residues. From 76% coverage of full-length Spd2, MS identified 28 *in vitro* Ser/Thr phosphorylated residues. The positions of the phospho-Ser/Thr residues are indicated in the Spd2 linear map. (B-D) *In vitro* kinase assays of purified His_6-tagged Plk4 kinase domain (amino acids 1-317) mixed with various Maltose-Binding Protein (MBP) and Glutathione -S-transferase (GST) Spd2 fusion proteins. The Coomassie-stained SDS-PAGE protein gels and their corresponding autoradiographs are shown. As expected, active Plk4 autophosphorylates (green arrowheads) but does not phosphorylate purified MBP (B) or GST (C, D). Plk4 does phosphorylate MBP- and GST-tagged-Spd2 fragments NT1 (B), NT2 (C), M and C (D) (red arrowheads). Some

proteolytic fragments of GST-Spd2-NT2 are visible and were phosphorylated. (E) RFP-Spd2 and endogenous Spd2 protein levels were analysed by immunoblotting lysate of larval brain extracts probed with Spd2 antibodies. (F) GFP-Spd2 and endogenous Spd2 protein levels were analyzed by immunoblotting lysate of S2 cells in a 7 day RNAi and replacement experiment. Transgenic GFP-Spd2 expression was induced with 0.5 mM CuSO4. Immunoblots were probed with anti-GFP and anti-Spd2 antibodies. *** represents a non-specific band recognized by the anti-GFP antibody. (G) Anti-GFP immunoprecipitates (IPs) were prepared from lysate of S2 cells transiently expressing the indicated combinations of GFP- and V5-Spd2 phosphomutants. Endogenous Spd2 was depleted using RNAi. Immunoblots were probed with anti-GFP and anti-V5 antibodies. (H) Anti-GFP immunoprecipitates (IPs) were prepared from lysate of S2 cells transiently expressing the indicated combinations of GFP-Spd2 phosphomutants and V5-Cnn. Endogenous Spd2 was depleted using RNAi. Immunoblots were probed with anti-GFP and anti-V5 antibodies.

SUPPLEMENTARY and MOVIE LEGENDS

Movie S1- Centriole behavior in Ctrl NBs

Related with Figure 1

Ctrl NB expressing Sas6 (in green) and α-tubulin (in red). Time is shown in minutes: seconds. Movie related to Fig. 1B. Centriole and centrosome behavior can also be followed with the tracking in the middle panel, which overlaps with a diagram where the apical position is on the top and on the tracking on the right panel, which overlaps with the movie shown on the left. Before the first mitosis, the apical centrosome (green full circle in the middle panel and empty blue circle on the right panel) and the basal centrosome (pink full circle in the middle panel and empty pink circle on the right panel) can be seen. After cytokinesis, only the apical centrosome is labeled as a full green circle and a blue empty circle on the middle and right panels respectively. At (T00.31min), the two centrioles disengage (pink full and empty circles in the middle and right panels label the basal centriole while a full green circle and a blue empty circle on the middle and right panels label the apical centriole).

Movie S2: Centriole behavior in Plk4^{KD} and Plk4^{WT} NBs

Related with Figure 1. This movie gathers three different movies from three

different NBs from the following genotypes: The first two are Plk4^{KD} expressing NB (in green) and the third is Plk4^{WT} expressing NB (in green). All NBs express α-tubulin (in red). Time is shown in minutes: seconds.

Movie S2A: from frame 2-192: Plk4^{KD} expressing NB- Centriole depicting apical behavior. Movie related to Fig. 1C. Centriole behavior can also be followed on the tracking in the middle panel, which overlaps with a diagram where the apical position is on the top and with the tracking on the right panel, which overlaps with the movie shown on the left. The apical centriole (blue full circle in the middle panel and empty blue circle on the right panel) can be seen oscillating in small trajectories always very close to the initial apical position throughout interphase. As mitosis starts (T114.00min), increased MT nucleation can be noticed and the amplitude of movements also increases. The spindle is initially nucleated from the centriole-containing pole, but a bipolar mitotic spindle is formed subsequently.

Movie S2B: from 193 to 326: Plk4^{KD} expressing NB- Centriole depicting apical mobile behavior. Movie related to Fig. 1D. Centriole behavior can also be followed on the tracking in the middle panel, which overlaps with a diagram where the apical position is on the top and with the tracking on the right panel, which overlaps with the movie shown on the left. The NB membrane is show as black empty circles in the middle and right panels. During interphase (from T6.00-57.00min), the apical centriole (blue full circle in the middle panel and empty blue circle on the right panel) is maintained closely associated with the apical cortex, even if displaying trajectories of larger amplitudes than the ones shown in Movie 2. Indeed the centriole moves laterally from one side of the cell to the other and it was thus named as apical mobile. Remarkably, even if the membrane of this NB is deformed, as the neighboring cell positioned above the apical cortex undergoes mitosis, the centriole is maintained associated with the apical hemisphere

Movie S2C: from frame 327 to 474: Plk4^{WT} expressing NB. Movie related to Fig. 1E. Centriole behavior can also be followed with the tracking in the middle panel, which overlaps with a diagram where the apical position is on the top and with the tracking on the right panel, which overlaps with the movie shown on the left. In Plk4^{WT}NBs, several centrosomes can be noticed. To facilitate comprehension, only one centrosome is shown in the tracking (full red circle in the middle panel and empty red circle on the right panel), which corresponds to the centrosome associated with the mitotic spindle pole

closer to the apical cortex at the end of mitosis (T00:21 min). This centrosome displays an erratic movement throughout interphase, while other centrosomes are also present and moving throughout the cytoplasm. On the following mitosis, two other centrosomes start to nucleate at an apical position, while the tracked centrosome does not nucleate MTs even if back to the apical hemisphere. Eventually, a bipolar spindle is assembled, without the participation of this centrosome, showing the loss of apical identity from the tracked centrosome.

Movie S3: Centriole behavior in Ctrl and Plk4^{KD} NBs after colcemid treatment
Related to Figures 2D-E. This movie gathers two different movies from two different NBs from the following genotypes after incubation with the MT depolymerizing drug colcemid. Ctrl NBs expressing Sas-6 GFP (in green) and Plk4^{KD} expressing NB (in green). All NBs express α-tubulin (in red). Time is shown in minutes: seconds.

Movie S3A: from frame 2-153- Ctrl NB after colcemid incubation-Movie related to Fig. 2D. Centriole behavior can be followed on the tracking in the middle panel, which overlaps with a diagram where the apical position is on the top and on the tracking on the right panel, which overlaps with the movie shown on the left. To facilitate comprehension, only the apical centriole is shown in the tracking (full red circle in the middle panel and empty red circle on the right panel). After disengagement (T-0.5min), the apical centriole moves initially towards the apical hemisphere and then to the basal hemisphere, where it remains till the following mitosis (T71.30min), where tubulin can be seen filling in the nuclear space. We noticed that in the presence of colcemid, the fluorescence intensity of Sas-6 signal decreases substantially when compared to controls.

Movie S3B: from frame 154-234- Plk4^{KD} expressing NBs after colcemid treatment. Movie related to Fig. 2E. Centriole behavior can be followed on the tracking in the middle panel, which overlaps with a diagram where the apical position is on the top and on the tracking on the right panel, which overlaps with the movie shown on the left. The centriole, which is shown in the tracking (full blue circle in the middle panel and empty blue circle on the right panel), remains initially associated with the apical hemisphere (until 16.00min), moves slightly towards the basal side, but remains more centrally located, never reaching the basal hemisphere as in the Ctrl with colcemid. We noticed that in the presence of colcemid, the GFP-Plk4^{KD} signal decreases substantially

when compared to controls. We confirmed that the centriole is still present and followed its behavior by increasing fluorescence intensity levels in order to generate the tracks.

Movie S4: Centriole behavior in Spd2^{WT}, Spd2^{DE} and Spd2^{AA} NBs

Related with Figure 4. This movie gathers three different movies from three different NBs from the following genotypes: Spd2^{WT}, Spd2^{DE} and Spd2^{AA} (in green). All NBs express α-tubulin (in red). Time is shown in minutes: seconds.

Movie S4A: from frame 2 to 247 Spd2^{WT} NB. Movie related to Fig. 4C. Centrosome and centriole behavior can be followed on the tracking in the middle panel, which overlaps with a diagram where the apical position is on the top and on the tracking on the right panel, which overlaps with the movie shown on the left. The apical centrosome, which is shown in the tracking (full blue circle in the middle panel and empty blue circle on the right panel), disengages at 42.00min. The apical centriole remains associated with the apical cortex, while the basal centriole is not detected throughout interphase, since it does not contain Spd2. At time 114min, the basal centrosome is detected at the basal hemisphere (full orange circle in the middle panel and empty blue circle on the right panel. In the following interphase, apical centriole disengagement occurs at 168min. The apical centriole is labeled as a full blue circle in the middle panel and an empty blue circle on the right panel, while the basal centrosome is labeled as a full green circle in the middle panel and an empty green circle on the right panel.

Movie S4B: from frame 248 to 406 Spd2^{DE}NB . Movie related to Fig. 4D. Centrosome and centriole behavior can be followed on the tracking in the middle panel, which overlaps with a diagram where the apical position is on the top and on the tracking on the right panel, which overlaps with the movie shown on the left. The apical centrosome, which is shown in the tracking (full red circle in the middle panel and empty red circle on the right panel), can be noticed during the initial phases of interphase and it disengages at (T19.00min) (the basal centriole is labeled as a full green circle in the middle panel and empty green circle on the right panel). Spd2DE signal is rapidly lost from the basal (T21.00min) and the apical centrioles (T23.00min). Throughout interphase, Spd2DE is not detected associated with the centrosomes, which most likely are mobile since centrosome association is noticed at the center and at the

basal side of the cell at (T11.00min) and (T121.00min) (full yellow circle in the middle panel and empty yellow circle on the right panel and full pink circle in the middle panel and empty pink circle on the right panel). The last centrosome to be detected and positioned at the basal side (pink in the tracking panels) moves towards the apical hemisphere as the mitotic spindle assembles. During interphase, certain regions with decreased fluorescence can be occasionally noticed like at (T56.00min), near the basal side of the hemisphere.

Movie S4C: from frame 407 to 533 $Spd2^{AA}$ NB expressing $Spd2^{AA}$ (in red) and α-tubulin (in green). $Spd2^{AA}$ signal is maintained at the centrioles throughout part of interphase. Time is shown in minutes: seconds. Movie related to Fig. 4C. Centrosome and centriole behavior can be followed on the tracking in the middle panel, which overlaps with a diagram where the apical position is on the top and on the tracking on the right panel, which overlaps with the movie shown on the left. The apical centrosome, which is shown in the tracking (full red circle in the middle panel and empty red circle on the right panel), can be noticed during the initial phases of interphase. Centriole disengagement is detected at 11.00min (one centriole is labeled in red while the other is labeled in orange) and both centrioles remain closer to the apical cortex until 44.00min. Only one centrosome (the one labeled in red) can be noticed until the following mitosis, where the second centrosome is again noticed on the basal side of the cell (time 94min).

Supplemental Table 1- In vitro phosphorylated residues of Spd2 (related with Figures 4-5 and Figure S6).

Spd2 was bacterially-expressed and purified as four fragments that, collectively, spanned the entire protein: MBP-Spd2-NT1 (amino acids 1-84), GST-Spd2-NT2 (amino acids 85-340), GST-Spd2-M (amino acids 341-662), and GST-Spd2-C (amino acids 663-1146). The Spd2 proteins were incubated with purified Plk4 kinase domain (amino acids 1-317) and MgATP, then resolved by SDS-PAGE, and the excised Spd2 bands processed for analysis by tandem mass spectrometry. Peptide sequences were identified with Sequest software. Confidence of the identification of the tryptic peptides was based primarily on Sequest Xcorr scores; a positive identification required an Xcorr score >1.5, >2.5 and >3.4 for singly, doubly and triply charged peptides, respectively. (This scheme was relaxed for the N-terminus [amino acids 1-340] because most candidate residues in this region did not display high probabilities [>95%] for both phosphate localization and peptide sequence.) Confidence of the peptide identification was further increased if the deltaCn score was >0.1. Probable phosphorylated residues are indicated with a box and were identified with Ascores and Phosphate Localization Probabilities (ScaffoldPTM, Proteome Software), using a phosphate localization probability of 95% as a threshold. (This scheme was relaxed for N-terminus residues.) No phosphorylated residues were observed in control samples of Spd2 (i.e., GST-Spd2 domains incubated with only MgATP prior to analysis). Coverage of Spd2 obtained from control GST-Spd2 samples: total = 77%, N-terminus (NT1+NT2) = 86%, M region = 83%, C-terminus = 68%. Coverage of Spd2 obtained from Plk4-treated GST-Spd2 samples: total = 78%, N-terminus = 83%, M region = 88%, C-terminus = 68%. Because of the proximity between S146 and S148 in the peptide sequence EKPSLSVAEIL from MBP-Spd2-NT1 with a Phosphate Localization Probability of 68%, we decided to mutagenize the two S encoding residues.

Residue	Peptide Sequence	Phosphate Localization Probability	Ascore	Peptide Score	Scaffold: Peptide Probability	Sequest : Xcorr	Sequest : DeltaCN	Sequest: Peptide RankSp	Sequest: PeptideSp	Charge
S34	GDL[S]SFSK	73%	7.38	51.74	69%	1.795	0.445	1	585.6	2
S35	VFGDLS[S]F	81%	6.20	26.57	46%	1.994	0.322	1	325	1
S92	LSTNI[S]ELVTDDTIDL	100%	22.93	69.11	80%	2.128	0.307	1	466	2
S121	GTNI[S]FEPAEITGR	100%	45.93	120.86	100%	3.88	0.492	1	731	2
S148	EKPSL[S]VAEIL	68%	3.34	29.68	75%	1.693	0.231	1	522.9	2
S191	GSSSSLSD[S]FNCSR	100%	41.42	120.89	100%	3.371	0.589	1	988.8	2
S239	AAEGQDESFAPAELMQ[S]K	100%	132.14	106.82	100%	3.05	0.425	1	915.8	2
S273	IAAPT[S]EIETSVSNSVL	90%	10.28	77.08	93%	2.462	0.553	1	378.2	2
S291	IAAPTSEIETSVSNSVLAGDPDF[S]L	100%	16.91	55.40	100%	2.705	0.43	1	783.8	2
S354	TDAITG[S]NLGR	100%	30.01	112.89	100%	2.85	0.478	1	344	2
T371	MQQDRIE[T]ALK	100%	1000.00	71.53	97%	2.768	0.399	1	117.1	2
S375	MQQDRIETALK[S]R	100%	53.61	56.24	93%	2.234	0.422	1	313.8	2
T384	NGLAAKE[T]KRPPSSSEILSLSAIDK	100%	24.19	45.65	100%	3.669	0.557	1	228.7	3
S391	RPPSS[S]EILSLSAIDK	98%	19.02	132.11	100%	3.178	0.471	1	674	2
S395	RPPSSSEIL[S]LSAIDK	100%	23.64	129.18	100%	4.204	0.632	1	276	2
S397	RPPSSSEILSL[S]AIDK	100%	51.96	97.15	100%	3.233	0.427	2	57	3
S443	GNNYDDGENKENQSSN[S]HAER	96%	12.63	70.12	100%	4.267	0.482	1	645.6	3
T458	LTD[T]MSFTDSVLNSTDFR	99%	22.30	162.62	100%	4.267	0.588	1	329	2

S460	LTDTM[S]FTDSVLNSTDFR	100%	28.23	117.63	100%	4.19	0.636	1	673.9	2
S464	LTDTMSFTD[S]VLNSTDFR	100%	44.44	115.08	100%	4.872	0.637	1	48	2
T493	KPLSPLADHPQI[T]ISR	100%	38.03	149.81	100%	4.014	0.539	1	479	3
S569	RV[S]IATMGLIPR	100%	47.36	101.72	100%	2.526	0.582	1	487.7	2
S673	GLGT[S]SVAVPR	96%	16.83	86.93	100%	3.042	0.476	1	442	2
T706	VTHT[T]LCWGSTK	100%	35.92	108.10	97%	2.627	0.499	1	527.5	2
T754	LGIQGPGFQLVGTDSSTI[T]LQAMECR	95%	10.21	15.97	98%	3.626	0.323	1	612.8	3
S949	EKLTSPMLD[S]IWGEFPDEQPVR	99%	17.35	115.47	99%	3.947	0.287	1	945.1	3
S1000	DFDESSES[S]LMFLPEADETVLFR	99%	19.02	91.50	100%	3.65	0.504	1	597.7	2